N O T I C E

THIS DOCUMENT HAS BEEN REPRODUCED FROM MICROFICHE. ALTHOUGH IT IS RECOGNIZED THAT CERTAIN PORTIONS ARE ILLEGIBLE, IT IS BEING RELEASED IN THE INTEREST OF MAKING AVAILABLE AS MUCH INFORMATION AS POSSIBLE

JPL PUBLICATION 80-20

Drag-Free Estimation Feasibility Study

Final Report

D.B. Schaechter
D.G. Carta
D. Noon
J. Parker
D. Sonnabend

(NASA-CR-163635) DRAG-FREE ESTIMATION FEASIBILITY STUDY Final Report (Jet Propulsion Lab.) 76 p CSCL 22B

N80-33454

Unclas
G3/15 29037

May 15, 1980

National Aeronautics and
Space Administration

Jet Propulsion Laboratory
California Institute of Technology
Pasadena, California

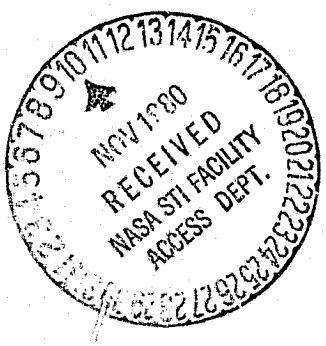

JPL PUBLICATION 80-20

Drag-Free Estimation Feasibility Study

Final Report

D.B. Schaechter
D.G. Carta
D. Noon
J. Parker
D. Sonnabend

May 15, 1980

National Aeronautics and
Space Administration

Jet Propulsion Laboratory
California Institute of Technology
Pasadena, California

The research described in this publication was carried out by the Jet Propulsion Laboratory, California Institute of Technology, under NASA Contract No. NAS7-100.

ABSTRACT

Complex spacecraft requiring a "drag-free" capability are often troubled by disturbances due to self-gravity and charge. To cope with these, estimation techniques, derived from modern control theory, have been proposed. This report presents the results of a study of the feasibility of applying those techniques. Throughout, special reference is made to the Solar Probe, a spacecraft for which these problems are regarded as unusually difficult. However, wide application of the technique to other missions is foreseen.

CONTENTS

PRECEDING PAGE BLANK NOT FILMED

FIGURES

1. INTRODUCTION AND SUMMARY

1.1 Statement of the Problem

Within the past few years, interest has grown in a close flight past the Sun—the Solar Probe. Amongst the mission objectives, a particular set is referred to here as "radiometric science". The set consists of all the scientific information that is potentially extractable from the Probe's orbit by DSN tracking. This includes the solar oblateness and other gravitational potential terms, measurement of some of the relativistic PPN parameters, and, possibly, the solar angular momentum.

Early in the mission design, it was recognized that uncertainties in the external forces, primarily solar pressure, would affect the orbit far more than the parameters that are intended to be measured. To circumvent this it was proposed to fly a drag compensation system. This is based on an instrument in which a small dense ball or "proof mass" floats free in a larger spherical cavity. Whenever the ball gets too close to the wall, an appropriately placed thruster is fired to keep the spacecraft away. Since the ball is protected from all external forces except gravity, it flies a "drag-free" orbit; and the spacecraft is never far behind. In 1973 this arrangement was flown aboard the navy TRIAD satellite and demonstrated drag compensation at the 10^{-10} m/sec^2 level (10^{-11} g), in spite of air drag and solar pressure effects that were orders of magnitude larger.

In Chapter 3 below, it will be shown that variations from a drag-free trajectory must be suppressed, or at least known, to within an overall error of 10^{-8} m/sec^2. This requirement could tighten, if better tracking is available than is there assumed. In Reference 1, it is shown that even the 10^{-8} m/sec^2 level isn't feasible without drag compensation. Early rough calculations along these lines, together with the known TRIAD performance, seemed to assure that the Solar Probe requirements could easily be met.

Unfortunately, the Solar Probe is a rather hostile environment for a drag-free instrument; and by mid-1978 it was widely perceived that the TRIAD design, as is, could not be counted on to perform, even at the 10^{-8} m/sec^2 level. One of the problems is self-gravity -- the gravitational attraction of the ball to every other part of the

spacecraft. On a rigid spacecraft, this effect could be balanced by a counterweight (as on TRIAD), or merely allowed for in analyzing the actual trajectory. On Solar Probe, however, articulated antennas and instruments, sloshing liquid propellant, and a thermally unstable main structure, all complicated the picture.

The other main problem is charge. Unpredictable levels of high-energy radiation can cause unsymmetrical charge transfer between the cavity walls and the proof mass. The resulting charge on the ball causes it to be attracted to the nearest wall. TRIAD did not suffer greatly from charge buildup, probably because its orbit was low enough to avoid most of the Van Allen radiation. However, some electrostatically supported gyros and accelerometers, with very similar geometries, have observed charge effects, both in orbit and in the laboratory. A recent estimate for Solar Probe (Reference 2), indicates that very severe charging could occur in both the Jovian and solar environments. In Chapter 2 below, it is shown that these levels are incompatible with even the relaxed performance requirement of 10^{-8} m/sec^2.

In late 1978 it was proposed to solve both of these problems by an application of estimation theory, together with a set of new on-board measurements. The proposal became RTOP 790-40-15 (-05), which was accepted, and funded equally from three NASA Divisions (Codes RSS, ST-5, and SC-7). This Final Report is the culmination of the resulting feasibility study.

The report is organized as follows. In the next section, an overview of estimation theory will be given, as applied to the present problem. Following that, the subject of in-flight calibration is introduced. This natural companion of estimation was not studied, due to lack of funds; but several ideas along this line were suggested by the study team members and are presented here. The introduction closes with a summary of the results and conclusions of the study.

Chapters 2-4 give a more detailed discussion in each of the three main areas of study — the on-board estimator, the ground estimation process, and the self-gravity model. In each case they were written by the team member who did most of the work. Because of the central role played by the drag compensation system in the Solar Probe

spacecraft and mission design, these three diverse views merit close attention by those directly concerned with the Solar Probe mission.

In retrospect, prior to this study, whether a drag compensation system was regarded as a tool for navigation, for aeronomy, or for the study of gravitational fields, it has widely been regarded as imposing very difficult constraints on the spacecraft and system design. The Solar Probe, by imposing its own barely tolerable constraints, has caused a rethinking of this position. The authors believe that the addition of estimation techniques to drag compensation systems will tend to cause them to be viewed as just another spacecraft system.

1.2 Estimation

Since the main tool for improving drag-free performance discussed here is estimation, and as the essential ideas are not widely known outside the controls field, this section is devoted to an exposition of those ideas. It is, however, confined to those aspects of the field that presently appear to be relevant to the drag-free problem.

To begin, suppose some physical process is thought to be described, with adequate accuracy, by a set of first order ordinary differential equations:

$$\dot{x} = F(x,t) + w(t) \tag{1}$$

Here, the vector x is referred to as the "state" of the system, the set of functions F are the known drivers of the process, and w is a random disturbance vector, for which some statistical information may be available. In controls jargon, w is referred to as "process noise".

Also, suppose that there exists a set z of measurements of the process, which can be modeled as:

$$z = H(x,t) + v(t) \tag{2}$$

in which the functions H are the known model of the measurements, and v is a random measurement noise vector, for which statistical information may exist.

Finally, suppose we were to build a model of the system. After deleting the unknown disturbance w from (1), that system could be integrated, yielding some supposed state history x(t). Putting this into (2), and ignoring the unknown noise v, a prediction of the measurements H(x,t), could be computed. Of course, even if the initial state x(0) were guessed perfectly, the prediction H would in general diverge from the actual measurements z(t).

In an "estimator", we put this divergence to work by feeding back the measurement discrepancy. Letting $\hat{x}$ be the "estimate" of x, an estimator based on (1) and (2) has this form:

$$\dot{\hat{x}} = F(\hat{x},t) + K(t)[z - H(\hat{x},t)] \tag{3}$$

where K is a rectangular matrix of time varying feedback gains. Loosely speaking, if it is possible to find gains K(t), such that except for w and v, $H(\hat{x},t) \to z$, and $\hat{x} \to x$, then the state x is said to be "observable" by the measurements z.

There are several possibilities for K. If the joint covariance of w and v is known, then K(t) may be derived from a theory due to R. E. Kalman, which strives to minimize the integrated, weighted covariance of $\hat{x} - x$. An estimator based on that theory is often called a "Kalman filter." In the case that F and H are not explicitly time dependent, and that w and v are stationary random processes, it often happens that the Kalman derived $K(t) \to K_\infty$ asymptotically, where K_∞ is a constant matrix. If K_∞ is used in (3), the estimator may be slow to converge; but it's much easier to build. For this reason, a constant K may be attempted, even if all this time independence and stationarity doesn't hold.

In some cases, a more sophisticated feedback is required than that allowed in (3). One form of this occurs when there are uncertain or slowly changing parameters in the F or H functions. Suppose α is a vector of these parameters. It is common practice to append α to x, and extend the state equations (1) by $\dot{\alpha} = 0$. The estimate $\hat{x}$ is extended in the same way by $\hat{\alpha}$, and the appropriate equations are appended to (3). This scheme permits a direct extension of Kalman theory to estimate α along with x, but there is no guarantee that the augmented state will continue to be observable.

More radical departures are possible in which the residuals $z - H(\hat{x},t)$ appear nonlinearly in (3). For instance, settling times can be improved at the cost of greater sensitivity to v and w by raising K when large residuals are encountered.

A more sophisticated technique is to regard large residuals as a symptom that the covariance of w and v has been underestimated. If this additional feedback is instituted, and K is continuously evaluated from Kalman theory, it will rise in response to increased residuals. These techniques for improving estimator performance, and others, are usually referred to as "adaptive" filters.

To see how all this applies to the present problem, consider the ground estimator for radiometric science. A possible (simplified, nonrelativistic) structure for this would use state variables

$$x = [\bar{R}, \bar{V}, \alpha] \tag{4}$$

where $\bar{R}$ and $\bar{V}$ are heliocentric position and velocity of the proof mass and α would include the scientific parameters of interest, uncertain parameters of the DSN, and suspected system biases. The state equations corresponding to (1) could then take the form:

$$\left.\begin{aligned} \dot{\bar{R}} &= \bar{V} \\ \dot{\bar{V}} &= \bar{g}(\bar{R},t) + \bar{f}(t) + \bar{w}(t) \\ \dot{\alpha} &= 0 \end{aligned}\right\} \tag{5}$$

Here $\bar{g}$ is the gravitational acceleration due to the Sun and planets, $\bar{f}$ is the combined self-gravity and charge disturbing acceleration as determined by the on-board estimator, and $\bar{w}(t)$ comprises the errors in both $\bar{f}$ and $\bar{g}$. An alternative formulation, in which $\bar{f}(t)$ is integrated on-board is discussed in Chapter 2 below, and is being actively considered. Whatever modifications to (5) are finally chosen, a ground estimator of the type (3) would get its measurements z from the DSN.

A structure similar to (5) for the ground estimator is analyzed in Chapter 3 below. It is shown there that for reasonable assumptions on the DSN measurement noise, the ability to extract J_2 of the Sun (a component of α) approaches its theoretical peak, provided the standard deviation on $\bar{w}(t)$, $\sigma_w \lesssim 10^{-8}$ m/sec^2.

However, possible improvements in the DSN, and the need to free more scientific parameters than just J_2, indicate that we should aim higher, i.e. $\sigma_w \lesssim 10^{-9}$ m/sec^2. Of course, individual contributions to the error in estimating $\bar{f}$ on board must be held on a still tighter leash.

Turning now to the on-board estimator, its purpose is to provide $\bar{f}$ in some form to the ground estimator. A number of conceptual difficulties make this problem harder than it at first appeared, so that even now, it is unclear what the state variables should be, or how the state equations (1) should look. Some of these difficulties will be touched on here — their resolution will have to await future effort.

The first problem is coordinate systems. Unlike the ground problem, there is nothing here even resembling inertial coordinates. Even the proof mass is acted on by the unknown $\bar{f}$, and it has no natural attitude reference. Perhaps best are cavity coordinates, where the origin is at the center of the cavity, and the axes are fixed in the instrument and aligned to the spacecraft attitude sensors. The most critical measurement is the position $\bar{r}_B$ of the proof mass in this system. It may be assumed that the rotation connecting cavity coordinates to the heliocentric coordinates of the ground estimator is available from the attitude determination system.

The utility of cavity coordinates is best seen by expanding $\bar{f}$ within them:

$$\bar{f} = \bar{a}_{SGO} + \bar{\bar{G}}_0 \bar{r}_B + \bar{a}_c(q, \bar{r}_B, V_i) \qquad (6)$$

Here, $\bar{a}_{SGO}$ is the acceleration that would be seen by the ball if it were centered in the cavity, $\bar{\bar{G}}_0$ is the tensor gradient of $\bar{a}_{SG}$ as seen at the center, and $\bar{a}_c$ is the electrostatic acceleration, shown as a function of the charge q on the ball, $\bar{r}_B$, and the set of potentials V_i of the plates in the cavity. That the two self-gravity terms used in (6) give sufficient accuracy is demonstrated in Chapter 4.

If $\bar{a}_c$ did not exist, it would be relatively straightforward to evaluate $\bar{f}$. A combination of pre-flight measurements, in-flight calibrations, and various on-board mass, motion, and temperature sensors could be used to determine $\bar{a}_{SGO}$ and $\bar{\bar{G}}_0$; and the proof mass position sensor of course measures $\bar{r}_B$. In part, the $\bar{a}_c$ term is difficult because its functional form is not yet established. Progress in this direction is reviewed in Chapter 2. A good deal of further work will be needed to complete this, and find reasonable approximations to the exact solutions.

Far more important is the fact that while $\bar{r}_B$ and the potentials V_i may be directly measured, there appears to be no simple way to determine q. Methods for discharging the proof mass are under development at Johns Hopkins University Applied Physics Lab; but there has been no testing and no publication of their analysis. A direct measurement of q by means of its effect on the cavity electric field has been suggested, but the precision needed for such a sensor at the largest q values makes this doubtful.

The approach discussed in Chapter 2 is simple — in principle. A set of six plates in the cavity are used as a position sensor in the TRIAD design. If time varying potentials V_i are applied to these plates, a motion of the proof mass will result, depending in part on $\bar{a}_c$. An analysis of this forced motion can presumably yield q. Theoretically, the best way to go about this is an estimator, in which q is one of the state variables, with the state equation $\dot{q} = 0$. The structure of the estimator would include the expressions (6), and would have to predict $\bar{r}_B$. The difficulty is that many other things contribute to $\bar{r}_B$ — attitude motions, center of mass shifts due to a variety of causes, external forces on the spacecraft, and thruster firings. A full treatment of all this might require an estimator of 20 states or more.

While the study is yet to be attempted, there is an excellent chance that all this

complication is unnecessary. Since the motion in all three axes is correlated, and as the different pairs of plates could be excited with different frequencies, and as these frequencies could be chosen to avoid other known motion frequencies, some of the drivers of $\bar{r}_B$ might be ignored. How many state variables could be deleted in this way, while retaining sufficient accuracy in the determination of q is not known. On the other hand, much of the estimation task just described is needed anyway for the spacecraft attitude determination system. Thus, a merging of the spacecraft drag-free and attitude estimators may be desirable. Much work will be needed to clarify all this.

1.3 In-Flight Calibration

Within the mathematical models used in the on-board and ground estimators, there are a number of fixed parameters; e.g., the self-gravity terms in $\bar{a}_{SGO}$ and $\bar{\bar{G}}_0$ that don't depend on moving or changing masses, and Earth ephemeris and tracking station location parameters. For many of these parameters, it is believed that the best a priori estimates of their values will be inadequate and that some kind of in-flight assessment is required. Indeed, in the ground estimator simulation discussed in Chapter 3 below, very modest Earth ephemeris errors completely prevented filter convergence.

Consider a parameter p appearing in either the ground or in-flight state equations (1), or in the measurement models (2). If there is reason to believe that p may change in flight, then it may be added to the state equations as $\dot{p} = 0$, and the estimator may be augmented as discussed in the last section. If a model for the variation of p exists, then we might improve this to $\dot{p}$ = model. On the other hand, if we are merely uncertain of the value of p, and don't believe it can change, we may opt for in-flight calibration. In this case, we pick a time when we are far from the Sun, and deliberately excite some motion such that the measured quantities will depend upon p, which is then estimated by the technique just discussed. During the critical parts of the mission, the augmentation is deleted from the estimator, and p is fixed at the value determined by calibration.

The obvious advantage of in-flight calibration of some parameters over continuing estimation is the smaller set of estimation equations during the critical parts of the mission. This is especially important for the on-board estimator; but even on the ground, the possibilities for reducing the a priori covariance of the Earth ephemeris and station location errors before perihelion passage are attractive. The expected worsening of doppler tracking near the Sun, due to coronal effects, adds importance to such a calibration.

The disadvantage of calibration is equally obvious -- for each calibrated

parameter it is necessary to justify the assumption of time invariance. To alleviate this somewhat, it is intended to have several calibration periods on both sides of perihelion. If a parameter changes significantly between calibrations, a post-flight correction may be possible.

It had been intended to investigate the possibilities for in-flight calibration during the present study, but lack of funds forced its deletion. Nevertheless, during the course of the study, a number of suggestions have been made. For example, the main self-gravity terms, $\bar{a}_{SGO}$ in (6), can be evaluated by flying drag-free for long periods far from the Sun, when little or no compensation will be needed. The solar pressure effects can be distinguished from outgassing and propellant leaks by rotating the spacecraft, and both can be distinguished from proof mass disturbances by ground tracking. The gradient terms $\bar{G}_0$ can be excited by articulating parts of the spacecraft, or modifying the drag compensation law, or both, to produce an $\bar{r}_B$ history that covers the cavity.

The suitability of the actual vector function $\bar{a}_c$ for charge effects in (6), and the parameters within it, can probably be established in ground test; however, a recalibration during flight is certainly desirable. During quiet parts of the mission, the charge q on the ball is liable to be small, especially if it has been recently uncaged. On the other hand, external forces will also be small, reducing interference due to unmodeled variations in $\bar{r}_B$. As a further aid in identification, excitation of any plate pair causes correlated motions in all three axes, a correlation which is increased if other plate pairs are excited at different frequencies. Calibration sensitivity can be further increased by operating with the ball quite close to the wall — sensitivity increases logarithmically with decreasing gap width.

Since the main on-board estimator has not yet been worked out, it is unclear, at this writing, whether the parameters in the spacecraft mass model

(mass, c.m., inertia tensor) will be individually observable. Certainly, any important effects due to articulated members can be seen by merely moving those members. Since many parameters are involved, much work will be needed to clarify this.

The biggest uncertainties in the charge estimation process probably lie in the solar pressure and propulsion models. To get solar pressure parameters, we will need calibration periods relatively close to the Sun, in which the shield is pointed at the Sun, and also displaced from it in both directions, for long enough to make the various effects observable. The possibility that changes in the shield's surface properties, near perihelion, may render calibration inadequate, must be seriously considered. As for propulsion parameters, the force and torque histories, during a firing of any thruster, can probably be deduced on-board by analysis of the $\ddot{r}_B$ data in an appropriately extended main estimator. Times remote from the Sun are probably best for this. However, to believe in this kind of a calibration, it will have to be shown that variations due to propellant temperature and catalytic bed history can be ignored, or at least adequately modeled.

Finally, there are some uncertain parameters in the ground filter. These include the ephemeris constants of the Earth's orbit, the ground station antenna locations, clock errors, doppler extractor biases, and the parameters of the coronal propagation model. For all but the last, some long drag-free periods, when little compensation is needed, could yield significant improvements. As for coronal problems, it is expected that a solar occultation will occur in the early portion of the trajectory. If so, it will permit a test of the propagation model, and a calibration of its parameters, under conditions similar to those at encounter.

As this discussion has shown, a great deal of work will be needed to design practical calibration sequences, investigate the observability of the parameters to be calibrated, simulate the process, and apply the results in

future system design iterations. The results will be critical in determining the accuracy with which we must measure the calibrated parameters before departure, and in working out mission sequencing and operations. They also provide necessary inputs to the science simulation for determining the overall performance in achieving the radiometric science objectives.

1.4 Summary of Results

The assumptions and results of the study are complex, and are dealt with in detail in the following chapters. Here is a distillation to give an overall feeling for the problem.

Chapter 2 deals mainly with the on-board estimator. A tentative structure was proposed and a covariance study was done, as with the ground estimator.

The main conclusions are:

- The estimator, limited by modeling errors below and complexity above, will probably be in the range of 10 to 20 states.
- The structure can be arranged to integrate the deviation between the actual and a truly drag-free trajectory. For white Gaussian modeling errors of 10^{-10} m/sec^2 in each axis, the covariance was integrated on a parabolic orbit, inside of 0.25 A.U. The results were errors in the deviation of 3-10 m at perihelion, and 100-300 m at the outbound end.

The charge problem is also addressed in Chapter 2. This includes charge-discharge mechanics, an electrostatic force model, and the design of a charge identification system.

The main findings are:

- Of all charging effects, the worst appears to be secondaries from external high-energy electrons. The worst time for this is likely to be Jupiter encounter, if no flare is active near the Sun. Near Jupiter, a ball charge of $\sim 10^{-9}$ coulomb is possible, leading to a potential of $\sim$20 kV. Spark discharges would probably prevent higher potentials in any case.
- Without charge identification, holding the acceleration due to this below 10^{-9} m/sec^2 requires that the charge should not exceed about 2×10^{-12} coulomb. Thus, either discharge to this level (about 40 V), or charge identification is required.

- No proven discharge technique appears to exist; but identification by electrostatic forcing and estimation looks feasible.

Chapter 3 looks at the ground estimator. A simplified Kalman filter was constructed and a covariance analysis was performed relating the tracking and drag-free estimation errors to the level of accomplishment of the radiometric science objectives. While, for simplicity, only the extraction of the solar J_2 was considered, many variations in the orbit, and the type and quality of tracking and drag-free data were studied. Here are some of the conclusions:

- The accuracy with which J_2 can be determined, σ_{J_2}, depends strongly on the orbit chosen. Quite apart from the obvious improvement from a closer perihelion, the orbit planned for Solar Probe at the time of this study was not the best for this purpose.
- At present levels of accuracy, range and angle information do little to augment the basic doppler tracking data; i.e., the filter runs nearly as well without them.
- If the doppler noise is taken as $\sigma_{\dot{r}} = 0.5$ mm/sec, then a drag-free estimation random error goal of 10^{-8} m/sec^2 (10^{-9}g) should be adopted. Drag-free errors smaller than this will not significantly reduce σ_{J_2}. However, a tighter goal should be set if a smaller $\sigma_{\dot{r}}$ can be assured.

Finally, Chapter 4 is concerned with the self-gravity model, particularly the effect of moving masses. For charge estimation, the center of mass is also a concern. Here are some results:

- Except for parts extremely close to the drag-free sensor, the effect of moving masses on the center of mass is more important than the change in self-gravity.
- Self-gravity variations due to high-gain antenna motion may be neglectable. The effect on the center mass is not.
- If the imaging instruments are articulated as a whole, the self-gravity variation is significant.

- Location of propellant to 1-2 cm is necessary for center of mass knowledge, and its mass must be known to better than 1 kg for self-gravity. A special tank will be needed for this.
- Thermal-structural stability of 1 cm or better is adequate to neglect self-gravity variations from this source. Much better stability is needed if center of mass variations are to be neglected, indicating that structural monitoring, by strain gauges, or temperature sensors, or both, will be needed.

It must be pointed out that most of these conclusions were derived from an overall drag-free estimation accuracy requirement of 10^{-8} m/sec^2, which came, in turn, from a doppler accuracy specification of 0.5 mm/sec. More accurate tracking systems, now being proposed, would tighten the drag-free accuracy, and the above conclusions.

It should also be pointed out that the work, on which most of this is based, simulated a filter in which the solar J_2 was the only quantity extracted. The actual filter will attempt to find several other parameters; e.g., relativity parameters and the solar angular momentum. The final variance for some of these parameters may prove to be more critically dependent on the drag-free data than is J_2. That is, estimation accuracy substantially better than 10^{-8} m/sec^2 may be desired, even if the doppler data is not improved.

2. ON-BOARD ESTIMATION

The on-board estimator for the Solar Probe has evolved from the following considerations:

1) What information can the ground estimation process best use?

2) What telemetry bandwidth is available for returning this information to Earth?

3) What estimator structure is feasible to implement in real time aboard a flight computer?

4) What information is available (either a priori or measured) to the on-board estimator?

Some of the results of this study have led to the following conclusions:

1) In order for the ground estimator to eliminate the effects of self-gravity and proof mass non-gravitational forces from the spacecraft trajectory, these forces, or the effect of these forces, must be obtained, along with their associated statistical covariance.

2) Due to the low bandwidth telemetry requirement of the Solar Probe, it is required that an averaged or integrated effect of the proof mass disturbances be radioed to Earth, rather than the raw sensor data.

3) Effort has been made to implement an estimator using linear system theory. This results in simple system models, and allows the wide body of knowledge pertaining to linear estimator theory to be applied. Since all computation must be performed in real time, the order of the estimator must be no larger than 10 to 20.

4) The on-board sensor information available to the estimator is the drag-free sensor, and any additional sensor information on the spacecraft mass distribution, charge, magnetic properties, etc.

2.1 Structure of the Estimator

A simple model for the proof mass disturbance evolves in the following digression. Consider an inertial frame of reference. (See Fig. 1) In this

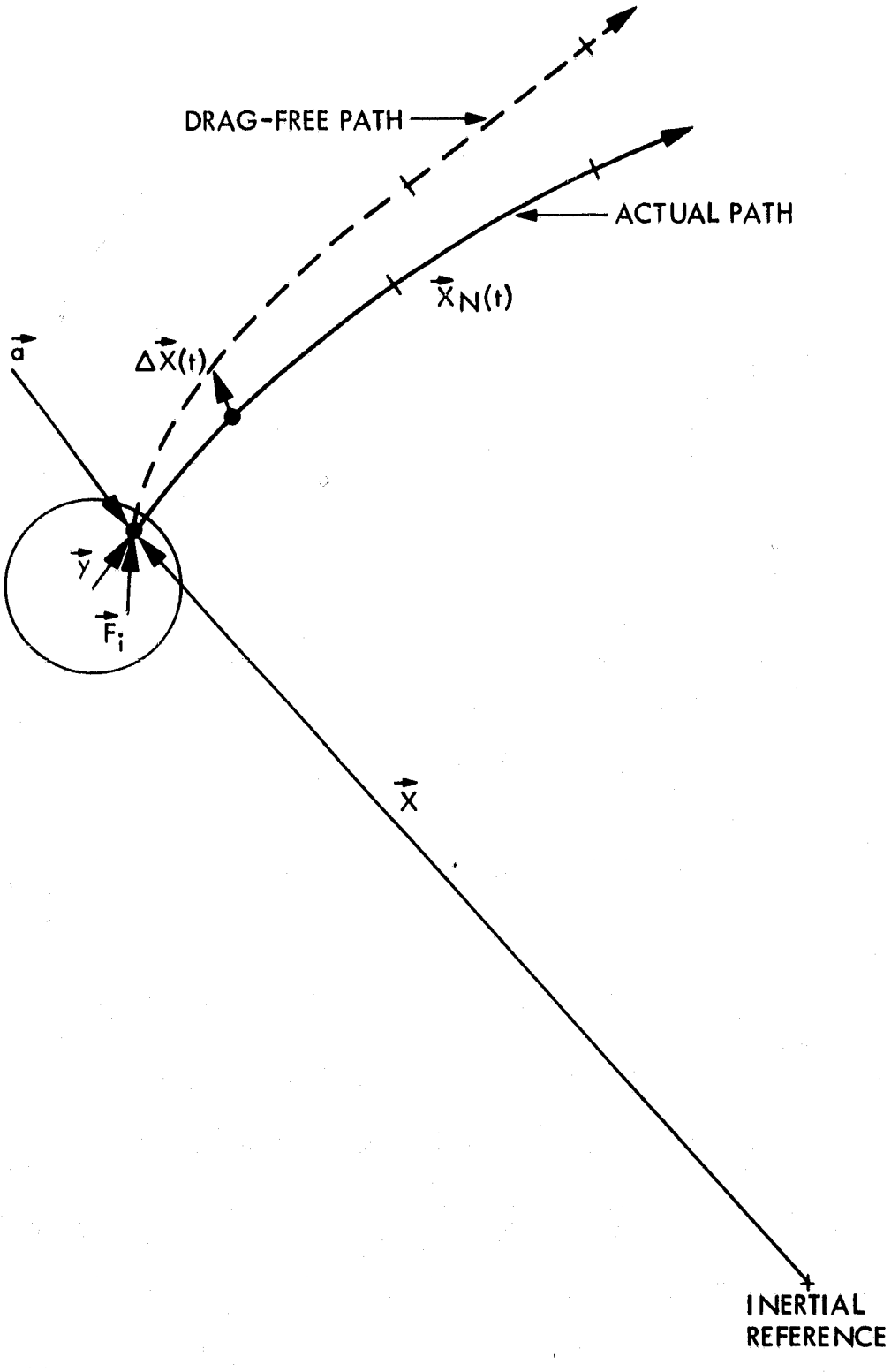

Figure 1. Spacecraft orbit variation.

reference frame, it is assumed that a model of the proof mass forces has been provided. This model will assume the following form when the drag-free control system is working properly:

$$\ddot{\vec{x}} = \vec{a} + \frac{\vec{F}_i}{m_{pm}} \tag{7}$$

where m_{pm} is the mass of the proof mass, $\vec{x}$ is the proof mass position relative to an inertial frame, $\vec{a}$ is the external gravitational acceleration, and $\vec{F}_i = m_{pm}\vec{f}_i$ is the internal force applied on the proof mass by portions of the spacecraft. In order to fly a drag-free orbit to a level required by the Solar Probe Mission, $\vec{f}_i$ must be known or estimated to high precision.

A more detailed examination of $\vec{f}_i$ now follows. $\vec{f}_i$ is composed of self-gravitational forces, electrostatic forces, magnetic forces, pickoff forces, brownian motion, etc., listed roughly in decreasing order of importance. With the use of a (perhaps 20th to 100th order) model of all the forces on the proof mass, and an inertial measurement of spacecraft position, it becomes possible to "fit" best coefficients to the modeled function form, e.g. to determine various gravitational harmonic coefficients of the Sun, and to distinguish these effects from self-gravitation forces and other internal forces. It is not realistic to assume that such a high-order estimation scheme can be implemented in real time using the on-board computer. At best, only 10 to 20 real time integrations should be assumed available.

However, this low bandwidth information is not actually required from the on-board estimator. Its purpose should be to provide the high bandwidth

information (which may have a non-zero averaged affect) to the ground estimator, either directly, or more desirably, in some integrated form. This latter scheme will be examined in greater detail.

2.2 Self-Gravity

In order to make the spacecraft a drag-free satellite, some effort is devoted to organizing the mass distribution of the satellite in a spherically symmetric configuration. However, due to initial calibration errors, fuel depletion, moving masses, thermal effects, etc., the net force and its gradient, at the center of the proof mass housing is not zero, and thus, drag-free errors are produced. The effects of these terms can be estimated using the following apprcach.

Consider the quantity $\vec{f}_i$, the internal spacecraft acceleration on the proof mass. It will be assumed that this acceleration can be represented in terms of the proof mass position in the cavity $\vec{y}$ and a vector of parameters $\vec{\alpha}$. $\vec{\alpha}$ may be composed of such things as boom extensions, hinge angles, proof mass charge, etc. So,

$$\vec{f}_i = \vec{f}_i(\vec{y}, \vec{\alpha}) \tag{8}$$

The perturbation effect of $\vec{f}_i$ on the nominal trajectory $\vec{x}_n(t)$ can be obtained by noting

$$\ddot{\vec{x}} = \vec{a}(\vec{x}) + \vec{f}_i(\vec{y}, \vec{\alpha}) \tag{9}$$

$$\ddot{\vec{x}}_n = \vec{a}(\vec{x}_n)$$

Letting $\Delta\vec{x} = \vec{x} - \vec{x}_n$, then

$$\Delta\ddot{\vec{x}} = \partial_{\vec{x}} \vec{a}(\vec{x}_n) \cdot \Delta\vec{x} + \vec{f}_i(\vec{y}, \vec{\alpha}) \tag{10}$$

The first term in (10) is the gradient of the external gravitational acceleration and can be accurately precalculated. The second term represents the effect of the perturbing internal forces. The second term can be further expanded by linearization of f_i about the point $(\vec{0},\vec{\alpha})$.

$$\ddot{\Delta x} = \partial_{\vec{x}} \vec{a}(\vec{x}_n) \cdot \Delta x + \vec{f}_i(\vec{0},\vec{\alpha}) + \partial_{\vec{y}} \vec{f}_i(\vec{0},\vec{\alpha}) \cdot \vec{y} + \text{HOT} \tag{11}$$

or using an appropriate notational substitution for simplicity

$$\ddot{\Delta \vec{x}} = \vec{\vec{G}}_x \cdot \Delta \vec{x} + \vec{f}_i(\vec{0},\vec{\alpha}) + \vec{\vec{G}}_y \cdot \vec{y} \tag{12}$$

A detailed explanation of each term of (12) follows:

- $\Delta \vec{x}$ is the vector difference between the actual flown path, and the "perfect" drag-free path. This is the quantity to be determined in real time aboard the spacecraft, and is of prime importance for correcting the actual trajectory flown to the estimated drag-free path.

- $\vec{\vec{G}}_x$ is a tensor (mainly the solar gravity gradient tensor) which includes the effects of the difference of gravity along the nominal trajectory from that along the actual drag-free trajectory. $\vec{\vec{G}}_x$ can be computed and stored in advance.

- $f_i(\vec{0},\vec{\alpha})$ is the total acceleration due to self-gravity, electrostatic forces, etc. at the center of the cavity. It looks like a bias, so there is no possibility for updating this value from its a priori computed value using a measurement $\vec{y}$ or $\vec{\alpha}$. The only possibility for obtaining $\vec{f}_i(\vec{0},\vec{\alpha})$ is through a measurement of $\Delta \vec{x}$. Furthermore, even with this measurement, $\vec{f}_i(\vec{0},\vec{\alpha})$ can only be distinguished if it looks different from, say, the solar gravity. By changing orientation of the spacecraft relative to the solar gravity vector, this discrimination is possible <u>but only if</u> inertial position information is available. This procedure may be used during a calibration phase of the mission.

Since the effects due to $\vec{f}_i(\vec{0},\vec{\alpha})$ are "slow," it would seem appropriate to allow these effects to be included in the ground estimation. This amounts to redefining a nominal trajectory which includes the effects of $\vec{f}_i(\vec{0},\vec{\alpha})$ and to let $\Delta\vec{x}$ now represent the departure away from this new nominal trajectory due to proof mass motion, $\vec{y}$, and changing spacecraft parameters, $\vec{\alpha}$.

Now, the equations of motion reduce to

$$\ddot{\Delta\vec{x}} = \ddot{G}_x \cdot \Delta\vec{x} + \ddot{G}_y \cdot \vec{y} \tag{13}$$

- $\ddot{G}_y$ is the self-gravity gradient at the center of the cavity. Note that spatial variation in $\ddot{G}_y$, as well as variations in $\ddot{G}_y$ due to changes in $\vec{\alpha}$ are both modeled here as higher order terms. $\ddot{G}_y$ can be computed in advance.

- $\vec{y}$ is the position of the proof mass relative to the cavity center. A measurement of $\vec{y}$ is available.

- $\vec{\alpha}$ is a vector of spacecraft parameters. If they are measured, they can be used as inputs to (13). If they are not measured, they can be assumed to be random disturbances acting on the proof mass.

At this point, it is worth pointing out that any a priori <u>known</u> inputs (such as antenna pointing angle) and their effects on the trajectory may be computed in advance and thus included in determining the nominal trajectory. Only effects which are not known a priori, such as fuel slosh, proof mass charge, thermal distortions, etc., need to be included in (13).

Equation (13) is easily put into state variable format

$$\frac{d}{dt}\begin{bmatrix}\Delta\vec{x} \\ \dot{\Delta\vec{x}}\end{bmatrix} = \begin{bmatrix}0 & I \\ \ddot{G}_x & 0\end{bmatrix}\begin{bmatrix}\Delta\vec{x} \\ \dot{\Delta\vec{x}}\end{bmatrix} + \begin{bmatrix}0 \\ \ddot{G}_y\end{bmatrix}\vec{y} \tag{14}$$

Inclusion of measurement error and process disturbance can also be included for determination of the variance of the state vector. It should be noted that without updates of the state from the ground, the variance of the state will continue to grow.

2.3 Charge Identification

After spacecraft self-gravity, proof mass electrostatic charge has the biggest impact on drag-free performance. Both the mechanism of proof mass charging, and the process of identifying proof mass charge will be analyzed. Reference 2 first showed how bad this could be for Solar Probe.

First, this section discusses some concepts of electrical charging of the Solar Probe drag-free mass resulting from penetration of energetic charged particles. The two portions of the mission of most concern are perijove and perihelion. The basic phenomenon of spacecraft charging involves the balance between the charged particle fluxes to and from (resulting from secondary emission processes) the spacecraft. A complete analysis of the problem requires knowledge of the energy spectrum of the particles as well as surface properties of the spacecraft. Analysis of charging internally also requires detailed knowledge of the spacecraft configuration.

The Pioneer model of the Jovian environment is satisfactory for determining charging effects during the perijove phase.[3] No satisfactory model exists for solar particles, but the Jovian environment can be taken as an upper bound.[4] No detailed configuration design exists for the Solar Probe, but estimates can be made on the basis of other spacecraft designs.

Reference 3 describes calculations on internal charging for the Galileo Jupiter Probe. Figure 2, taken from that report, shows some of the results. The broken curve represents potentials on the internal aluminum structure and

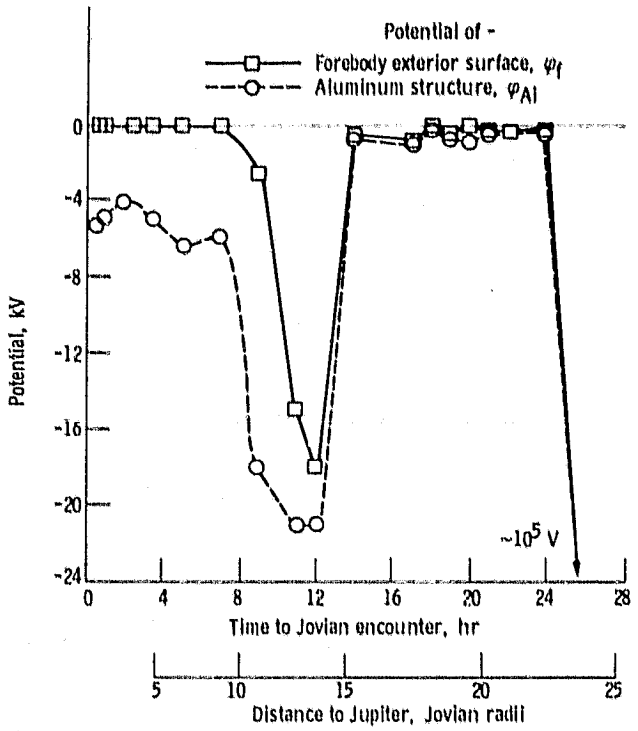

Figure 2. Potentials attained by probe forebody.

should be representative of internal charging levels in the neighborhood of Jupiter. No secondary electron emission from the aluminum structure was included. If the drag-free mass is treated as an isolated spherical capacitor, 20 keV implies a free charge of $\sim 10^{-9}$ coulombs on it. Inclusion of secondary emission would probably lower this by a factor of 10 to 100.

The response time of the ball will depend on both the environmental fluctuations and the natural leakage from the ball. Since most environmental changes are probably slow compared to the time constant of the ball, the charging process should follow the environment for <u>increasing</u> charging levels. However, if the ball is well isolated (e.g., very low residual gas surrounding it) the decay time should be very long (hours?).

Alternatively, it will be necessary to provide some continuous leakage path between the ball and cavity. For example, a low-pressure electronegative gas such as SF_6 could perhaps scavenge free charge from the sphere and deposit it somewhere on the cavity surface or vice versa. A more refined analysis must await a detailed specification of the spacecraft configuration. In fact, a maximum charge level on the drag-free mass could be made a design requirement.

Putting aside the proof mass charging mechanism, the effects and identification of proof mass charge are yet to be resolved.

Consider the arrangement shown in Figure 3. A proof mass of radius a is displaced a distance x from the center of the cavity of radius b.

Regarding the inside of the cavity as a complete spherical conductor, the ball-to-wall capacitance has been shown to be [5,6] approximately

$$C = 4\pi\varepsilon_o b\left[\frac{\lambda}{2\alpha}\ln\left(\frac{1+\alpha}{1-\alpha}\right) - 1\right] \tag{15}$$

where $\lambda = \frac{b}{b-a}$; $\alpha = \frac{x}{b-a}$ (16)

and ε_o = 8.85 x 10^{-12} Farad/m = permitivity of free space. Also the gradient of C in the direction of the displacement is:

$$\frac{dC}{dx} = \frac{2\pi\varepsilon_o\lambda^2}{\alpha}\left[\frac{2}{1-\alpha^2} - \frac{1}{\alpha}\ln\left(\frac{1+\alpha}{1-\alpha}\right)\right] \tag{17}$$

In the present Solar Probe design, a = .011 m and b = .02 m, giving λ = 2.22. Then, if the ball is displaced half way to the wall, x = .0045 m and α = 0.5, from which C = 3.21 x 10^{-12} Farad and dC/dx = 2.58 x 10^{-10} Farad/m.

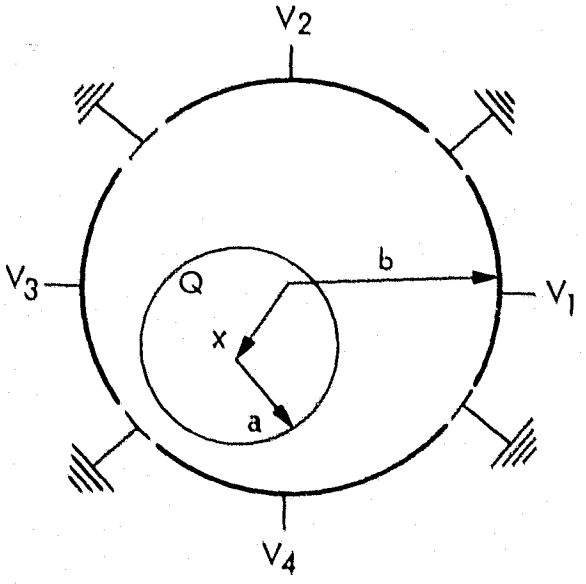

Figure 3. Proof mass and proof mass housing model.

Now, if the proof mass carries an absolute charge q, it is not hard to show that it is attracted to the nearest point on the wall by a force

$$F = \frac{q^2}{2C^2} \frac{dC}{dx} \tag{18}$$

Thus, if there is a maximum tolerable disturbing acceleration A, then the tolerable charge is

$$|q| < C\sqrt{2m_{pm}A\left(\frac{dC}{dx}\right)^{-1}} \tag{19}$$

Well, a 70% gold, 30% platinum ball has a specific gravity of 20, and thus, $m_{pm} = 0.112$ kg. Then, for $A = 10^{-10}$ m/sec^2, we get $|q| < 9.43 \times 10^{-13}$ coulomb. Since this is well below the expected levels, something must be done.

A possible approach to this is to apply varying voltages to the sensor plates, and thus, excite a motion proportional to q. By observing the actual motion, we can hope to identify q by estimation. To examine this, suppose for simplicity that the proof mass is centered, and that a voltage $\pm$ v is applied to a pair of opposing plates. Then the absolute proof mass potential is q/C, and the force on it can be shown to be[6]

$$F = \frac{1}{2}\left[\left(\frac{q}{C} + v\right)^2 - \left(\frac{q}{C} - v\right)^2\right]\frac{dC_P}{dx} = \frac{2qv}{C}\frac{dC_P}{dx} \tag{20}$$

Here C is found from (15) with $\alpha = 0$:

$$C = 4\pi\varepsilon_0 a\lambda \tag{21}$$

while C_p is the capacitance from the ball to one sensor plate:

$$C_p = 2\pi\varepsilon_o a\lambda(1 - c\theta); \quad \frac{dC_p}{dx} = \pi\varepsilon_o \lambda^2 s^2\theta \tag{22}$$

where θ is the half cone angle subtended by the sensor plate at the center of the cavity. For θ = 35 deg and the above dimensions, $C = 2.72 \times 10^{-12}$ Farad, $C_p = 2.46 \times 10^{-13}$ Farad, and $dC_p/dx = 4.52 \times 10^{-11}$ Farad/m.

Now, if this applied voltage is taken as sinusoidal:

$$v = v_o\, s(\omega t) \tag{23}$$

then, from (20), the amplitude of the induced motion is:

$$x_m = \frac{2qv_o}{m_{pm}\omega^2 C}\,\frac{dC_p}{dx} \tag{24}$$

Then if $v_o = 10^3$ volts, ω = 1 radian/sec, and q is the maximum tolerable value from (19), we get $x_m = 2.71 \times 10^{-7}$ m.

While this level of resolution in the proof mass position sensor would be very difficult to obtain, there are several possibilities for relaxing the requirement. First, the ball and cavity dimensions are not yet fixed, and could be adjusted to increase x_m. Second, a higher v_o or a lower ω may be possible. Third, a square wave excitation in place of the sinusoid

(23) would be helpful. Fourth, sensitivity can be improved by exciting all three pairs of sensor plates at different frequencies. Finally, the estimator bandwidth could be reduced by lowering the feedback gains, thus, averaging the sensor noise. If, say, 1 hour of settling is allowed with this ω, the required sensor resolution could be increased by a factor of around 60, or 1.6×10^{-5} m with the above numbers. This level was achieved on TRIAD. While this discussion does not constitute a design, it seems clear that charge identification by estimation is feasible.

2.4 Estimator Design and Variance Propagation

The real time integration of the vector equation 13 in Section 2.3 requires that these equations be resolved in some suitable reference frame. With this accomplished, a nominal spacecraft trajectory and a statistical description of the proof mass disturbance forces are sufficient to propagate the covariance of the estimated correction to the position and velocity of the Solar Probe through the solar encounter. Recall that this information, along with the position and velocity corrections themselves, is precisely what is needed by the ground estimator to improve the drag-free trajectory knowledge. The analytical approach may be summed up as

follows. A dynamic model of the perturbed trajectory of the Solar Probe away from an exact drag-free path is obtained in terms of random disturbances. The vector equations are resolved in a Euler-Hill accelerated frame (see Fig. 4) since 1) the solar gravity gradient is easily written in this frame and 2) the spacecraft maintains a fixed orientation in this frame through solar encounter and hence the statistics of many of the random disturbances are likely to be constant. These are the equations which will be integrated on-line aboard the spacecraft. The propagation of the radial, in-track, and cross-track position and velocity variances are obtained for unit variance acceleration inputs. Since the dynamic equations are linear, the resulting covariances may be scaled and added to fit the actual statistics of the disturbance environment.

The unperturbed equation of motion of the Solar Probe can be written in vector form as

$$\ddot{\vec{R}} = \vec{a}(\vec{R}) \tag{25}$$

where $\vec{a}$ is the external gravitational acceleration and $\vec{R}$ is the position vector of the unperturbed position of the solar probe relative to the sun.

Due to random disturbances $\vec{f}_d$, the actual position of the spacecraft, and the dynamic equation of motion can be written

$$\ddot{\vec{R}} + \ddot{\vec{r}} = \vec{a}(\vec{R} + \vec{r}) + \vec{f}_d \tag{26}$$

The vector difference of (13) and (12) yield

$$\ddot{\vec{r}} = \frac{\partial \vec{a}}{\partial \vec{R}} \cdot \vec{r} + \vec{f}_d \tag{27}$$

Equation (27) is the perturbation dynamic equation of motion. The natural dynamics are due to the solar gravity gradient $(\frac{\partial \vec{a}}{\partial \vec{R}})$ and the forced behavior is due to the proof mass disturbance.

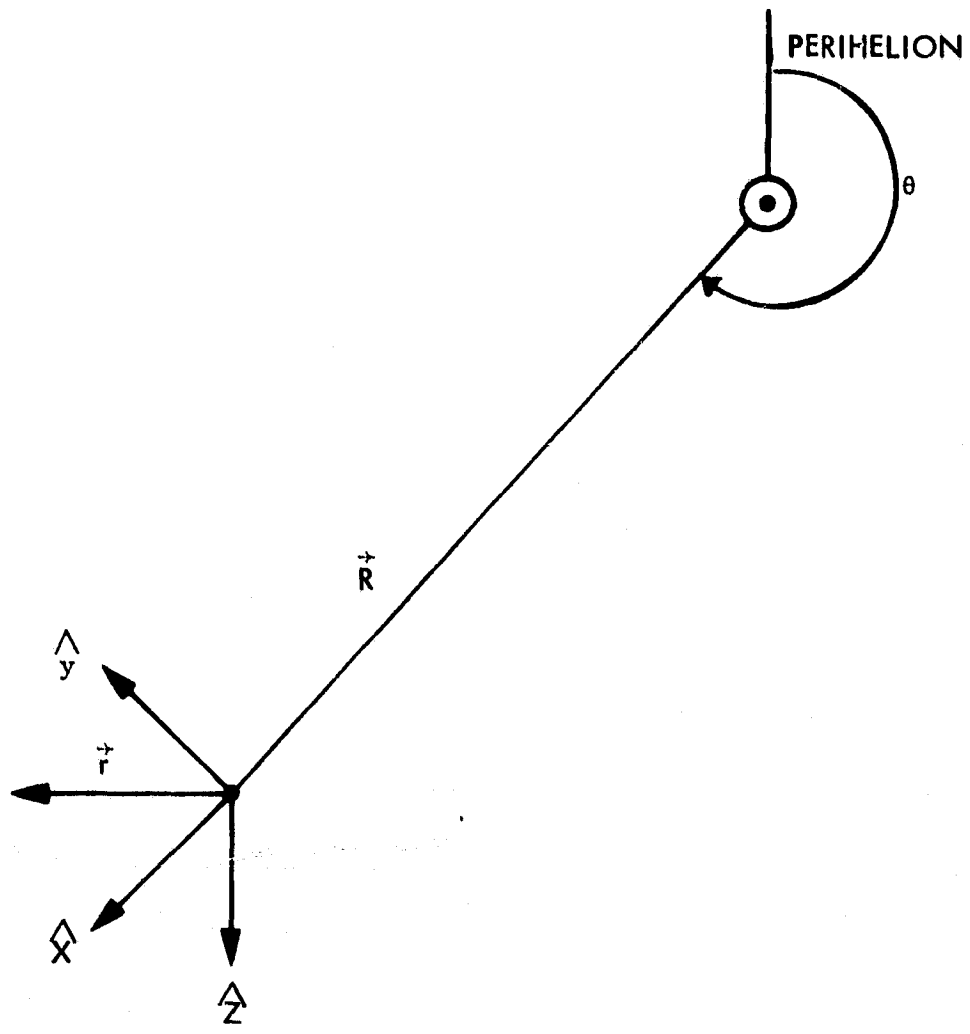

$\hat{x}$ is the radial direction

$\hat{z}$ is perpendicular to the orbit plane in the direction of the orbital angular momentum vector

$\hat{y}$ is $\hat{z} \times \hat{x}$

Figure 4. Euler-Hill coordinate frame.

The solar gravity gradient in the Euler-Hill coordinate system of Figure 4 is easily shown to be

$$\frac{\partial \vec{a}}{\partial \vec{R}} = \frac{\mu_\odot}{R^3} \begin{bmatrix} 2 & 0 & 0 \\ 0 & -1 & 0 \\ 0 & 0 & -1 \end{bmatrix} \tag{28}$$

where $R = |\vec{R}|$

and the disturbance force and position vector become:

$$\vec{f}_d = \begin{bmatrix} f_x \\ f_y \\ f_z \end{bmatrix} \qquad \text{and} \qquad \vec{r} = \begin{bmatrix} x \\ y \\ z \end{bmatrix} \tag{29}$$

Since the accelerations are measured in an accelerated reference frame, kinematics must be used to derive the following result:

$$\ddot{\vec{r}} = \begin{bmatrix} \ddot{x} - 2\omega\dot{y} - \omega^2 x - \alpha y \\ \ddot{y} + 2\omega\dot{x} - \omega^2 y + \alpha x \\ \ddot{z} \end{bmatrix} \tag{30}$$

where $\omega = \dot{\theta}$ is the angular velocity of the reference frame (and also the angular velocity of the unperturbed satellite position about the Sun)

and $\alpha = \ddot{\theta}$ is the angular acceleration of the reference frame (and also the angular acceleration of the unperturbed satellite position about the Sun)

From orbital mechanics, R, ω, and α can all be obtained as a function of the angular position of the satellite from perihelion, θ.

The two basic equations used are

$$R = \frac{p}{1 + e \cos \theta} \tag{31}$$

$$R^2\dot{\theta} = h = \sqrt{\mu_o p} \tag{32}$$

Equation (31) is the polar equation of a conic section in terms of two known constants p, the semilatus rectum, and e, the eccentricity of the orbit. p depends only on the known orbit angular momentum about the Sun, h.

Equation (32) is the statement that the angular momentum of the unperturbed orbit, h, is a constant.

From (31) and (32), and defining a new known constant N to be $\frac{\mu_o}{p^3}$ (not the mean motion)

$$\omega = \dot{\theta} = N(1 + e \cos \theta)^2 \tag{33}$$

$$\alpha = \ddot{\theta} = \omega \frac{d\omega}{d\theta} = - 2 N^2 e(1 + e \cos \theta)^3 \sin \theta \tag{34}$$

$$\Gamma = \frac{\mu_o}{R^3} = N^2(1 + e \cos \theta)^3 \tag{35}$$

Collecting the results thus far, equation (27) in the Euler-Hill reference frame can be written

$$\begin{aligned} \ddot{x} - 2\omega \dot{y} - (\omega^2 + 2\Gamma)x - \alpha y &= f_x \\ \ddot{y} + 2\omega \dot{x} - (\omega^2 - \Gamma)y + \alpha x &= f_y \\ \ddot{z} + \Gamma z &= f_z \end{aligned} \tag{36}$$

Furthermore, by rescaling the time variable so that

$$N \frac{dx}{d\tau} = \frac{dx}{dt} \tag{37}$$

the equations can be condensed to state variable form.

$$\frac{d}{dt}\begin{bmatrix} x \\ x' \\ y \\ y' \\ z \\ z' \end{bmatrix} = \begin{bmatrix} 0 & 1 & 0 & 0 & 0 & 0 \\ \omega^{*2}+2\Gamma^* & 0 & \alpha^* & 2\omega^* & 0 & 0 \\ 0 & 0 & 0 & 1 & 0 & 0 \\ -\alpha^* & -2\omega^* & \omega^{*2}-\Gamma^* & 0 & 0 & 0 \\ 0 & 0 & 0 & 0 & 0 & 1 \\ 0 & 0 & 0 & 0 & -\Gamma^* & 0 \end{bmatrix} \begin{bmatrix} x \\ x' \\ y \\ y' \\ z \\ z' \end{bmatrix} + \begin{bmatrix} 0 \\ f_x^* \\ 0 \\ f_y^* \\ 0 \\ f_z^* \end{bmatrix} \qquad (38)$$

where $(\,)'$ denotes $\frac{d(\,)}{d\tau}$, $f_i^* = f_i/N^2$, and

$$\omega^* = (1 + e\cos\theta)^2$$

$$\alpha^* = -2e(1 + e\cos\theta)^3 \sin\theta$$

$$\Gamma^* = (1 + e\cos\theta)^3$$

These are the equations which must be integrated aboard the spacecraft in real time. The input forces are those obtained from knowledge of the proof mass position, the satellite mass distribution, and the proof mass charge. Note that ω^*, α^*, and Γ^* can all be precomputed along the nominal spacecraft trajectory. For the present discussion, assuming the f*'s random variables, and perfect initial state information, it is possible to propagate the the covariance of the state error through encounter by using

$$X' = FX + XF^T + Q \qquad X(0) = 0 \qquad (39)$$

where X is the covariance of the state error, and Q is the spectral density of the disturbances.

A final change of variables from scaled time τ to θ yields

$$\frac{dX(\theta)}{d\theta} = \frac{1}{\omega(\theta)}\left[F(\theta)X(\theta) + X(\theta)F^T(\theta) + Q(\theta)\right] \qquad X(\theta_o) = 0 \qquad (40)$$

Equation (40) is linear in Q (the forcing function) and so X may be obtained for general inputs by superposition of the unit solutions for

$Q(2,2) = 1$

$Q(4,4) = 1$

$Q(6,6) = 1$

The nominal trajectory studied was an orbit of 0.02 AU perihelion and eccentricity 1.0. This results in a convenient value of $N^2 \sim 10^{-10}/sec^2$ The covariances were propagated from - 1/4 AU to + 1/4 AU, i.e., through solar encounter and the unit solutions are shown in Figures 5, 6, and 7. Note the somewhat strange behavior of all the covariances. The wiggles are due to the rapidly changing orientation of the reference frame.

As a scale, a random radial acceleration of 10^{-10} m/sec^2 acting through the entire solar encounter phase with exactly known initial conditions at the start of solar encounter propagates to a 100-meter uncertainty in drag-free position along the $\hat{y}$ coordinate.

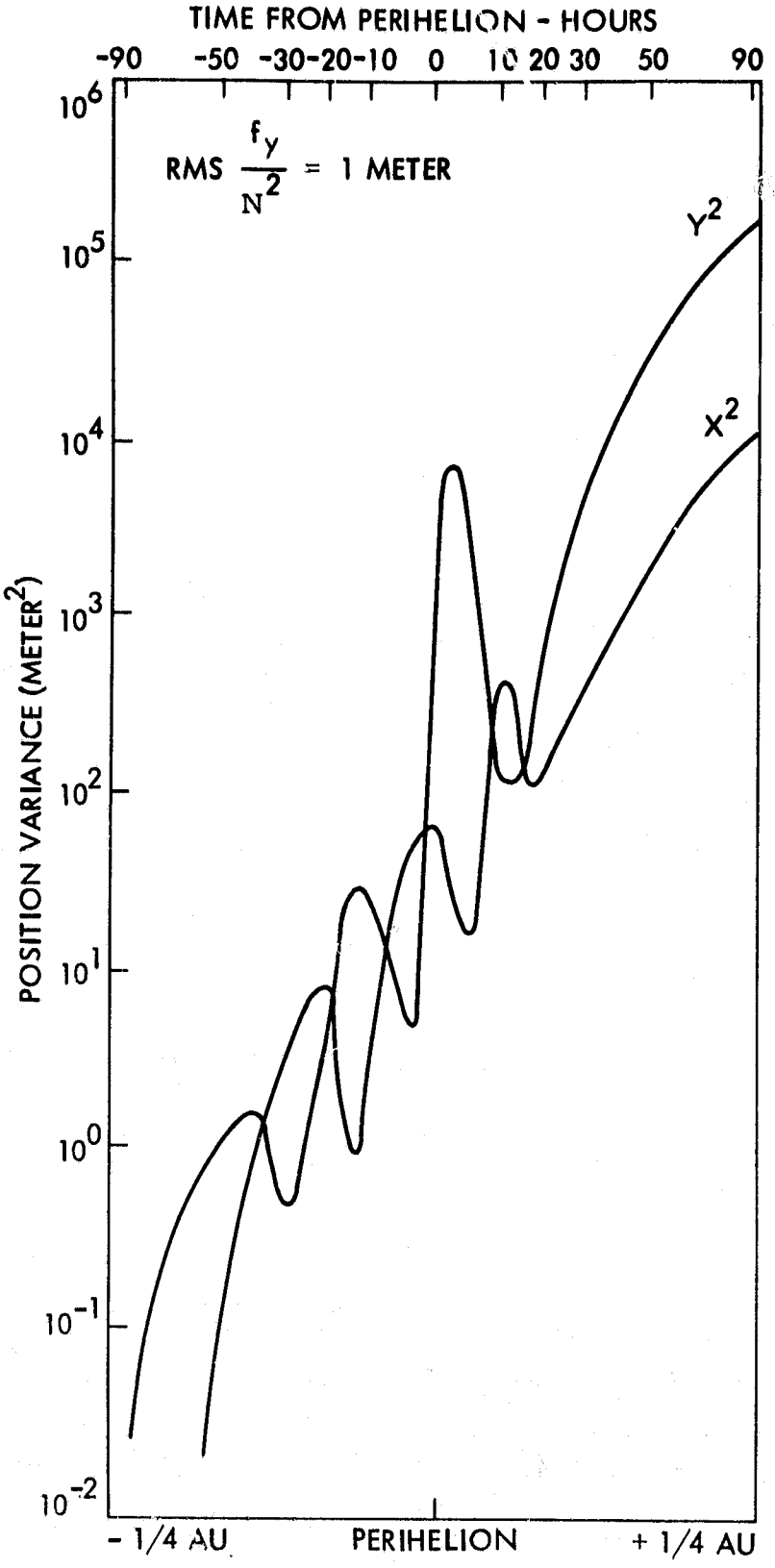

Figure 5. Trajectory uncertainties due to X disturbance.

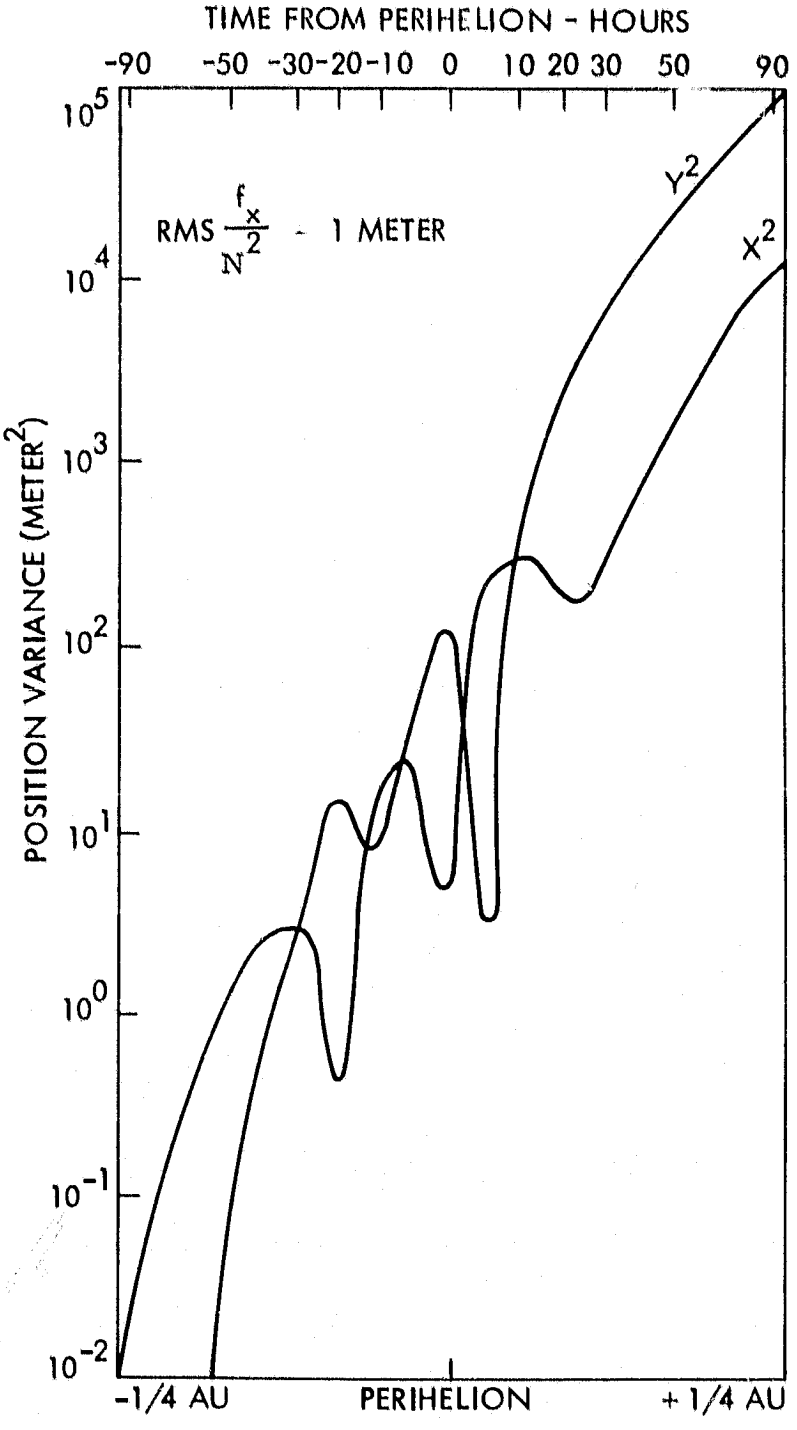

Figure 6. Trajectory uncertainties due to Y disturbance.

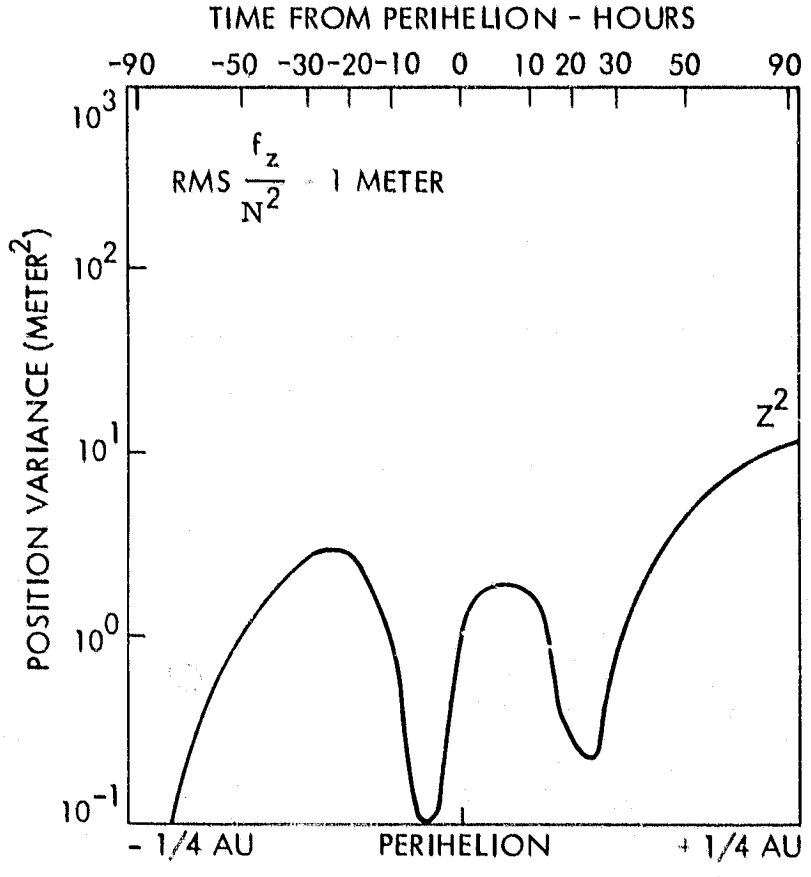

Figure 7. Trajectory uncertainties due to Z disturbance.

3. GROUND ESTIMATION

3.1 Objective

Major radiometric objectives of the Solar Probe mission will be to extract the relativistic parameters γ and β, and the quadrupole moment of the Sun, J_2. In this report, attention has been directed to the estimation of J_2. This estimation will be performed by accurately determining the trajectory of the spacecraft and relating the deviation from the pure inverse square gravitational path to the effect attributable to J_2.

To this end, a ground estimator will be constructed which mathematically links J_2 to the trajectory. Since the estimation will be based on observations of the spacecraft from the Earth, an optimal estimator of the Kalman type is indicated.

In order to determine to what accuracy J_2 might be calculated, a simulation was performed. Because only the variance of J_2 is required, and it will be extracted from the trajectory, only major contributions to the trajectory behavior need be considered in the simulation. The actual estimator will, of course, be required to account for all known effects.

3.2 Structure of the Estimator

An ordinary Kalman filter was implemented to perform the estimation. The model used for state updating is the Taylor series expansion for the position $\underline{r}_k$ and velocity $\dot{\underline{r}}_k$ of the probe relative to the Sun augmented by an equation expressing our expectation that J_2 will remain approximately constant. Thus we have

$$\underline{r}_k = \underline{r}_{k-1} + D\dot{\underline{r}}_{k-1} + \frac{1}{2} D^2 \ddot{\underline{r}}_k + \frac{1}{6} D^3 \dddot{\underline{r}}_k + \frac{1}{2} D^2 \underline{u}_k \tag{41}$$

$$\dot{\underline{r}}_k = \dot{\underline{r}}_{k-1} + D\ddot{\underline{r}}_k + \frac{1}{2} D^2 \dddot{\underline{r}}_k + D\underline{u}_k$$

$$J_k = J_{k-1} + w_k$$

where D is the time interval between updates, and $\ddot{\underline{r}}_k$ and $\dddot{\underline{r}}_k$ are derived from the solar gravity potential. The notation $(\underline{r}_k)_1 = x$, $(\underline{r}_k)_2 = y$, $(\underline{r}_k)_3 = z$, $r = (x^2 + y^2 + z^2)^{\frac{1}{2}}$, and $(J_2)_k = J_k$ is used.

Stochastic forces $\underline{u}_k$ are assumed to perturb the spacecraft motion. These forces arise through deviations from drag-free performance attributable to spacecraft self-gravitational forces and electromagnetic disturbances to the proof mass. The $\underline{u}_k$ force can also have a component of "force" associated with model truncation errors or mismodelling of other gravitational sources such as planets.

For the solar gravitational potential

$$\ddot{x} = -\frac{Gm\,x}{r^3}\left[1 + \frac{3}{2}J_2\frac{r_s^2}{r^2}\left(1 - 5\frac{z^2}{r^2}\right)\right] \tag{42}$$

$$\ddot{y} = -\frac{Gm\,y}{r^3}\left[1 + \frac{3}{2}J_2\frac{r_s^2}{r^2}\left(1 - 5\frac{z^2}{r^2}\right)\right]$$

$$\ddot{z} = -\frac{Gm\,z}{r^3}\left[1 + \frac{3}{2}J_2\frac{r_s^2}{r^2}\left(3 - 5\frac{z^2}{r^2}\right)\right]$$

where r_s = solar radius = 6.96×10^5 km, and

$$\dddot{x} = -\frac{Gm}{r^5}\left[\dot{x}(r^2-3x^2) + \dot{y}(-3xy) + \dot{z}(-3xz)\right] \tag{43}$$

$$\dddot{y} = -\frac{Gm}{r^5}\left[\dot{x}(-3xy) + \dot{y}(r^2-3y^2) + \dot{z}(-3yz)\right]$$

$$\dddot{z} = -\frac{Gm}{r^5}\left[\dot{x}(-3xz) + \dot{y}(-3yz) + \dot{z}(r^2-3z^2)\right]$$

Terms in J_2 have been omitted above because of their negligible effect at this level of expansion. (For the Sun, $J_2 = O(10^{-7})$).

3.3 Data and Trajectories

The estimator is able to process as observables simulated spacecraft range, range rate, and angular position measurements obtained from a single station located at 45° N Latitude. Observations are generated regularly at one minute intervals. For purposes of this simulation, the earth is assumed to be transparent. The measurement equations are

Range

$$z_1 = |\Delta \underline{r}| + v_1 \qquad \sigma_{v_1} = 25 \text{ m} \tag{44}$$

Range Rate

$$z_2 = \frac{\Delta \underline{r} \cdot \Delta \underline{r}}{|\Delta r|} + v_2 \qquad \sigma_{v_2} = 0.5 \text{ mm/sec}$$

Angular

$$z_3 = \tan^{-1}\left[\frac{\Delta r_y}{\Delta r_x}\right] + v_3 \qquad \sigma_{v_3} = 0.05 \text{ μrad}$$

$$z_4 = \tan^{-1}\left[\frac{\Delta z}{\left(\Delta r_x^2 + \Delta r_y^2\right)^{1/2}}\right] + v_4 \qquad \sigma_{v_4} = 0.05 \text{ μrad}$$

where $\Delta \underline{r}^T = [x, y, z,]_{\text{probe}} - [x, y, z]_{\text{Earth}}$

The above σ's are consistent with current expectations for accuracies achievable with radiometric observables in the late 1980's. The values for σ_{v_3} and σ_{v_4} correspond to the accuracies achievable through an operational ΔVLBI system as now contemplated for the Galileo mission. A discussion of possible impediments to obtaining the indicated accuracy for the range rate measurement occurs later.

The initial value for the state covariance matrix P as required by the Kalman filter was chosen as follows:

$$P_o = \text{diag}\ (\sigma_p^2,\ \sigma_p^2,\ \sigma_p^2,\ \sigma_v^2,\ \sigma_v^2,\ \sigma_v^2,\ \sigma_J^2) \tag{45}$$

where σ_p = 10 km, σ_v = 10 cm/sec, and $\sigma_J = 10^{-6}$.

The above accuracies are easily achievable by the usual tracking algorithms in use today, and can be generated well before solar encounter. While this a priori σ_J is questionable, it will be seen that the important results are not very sensitive to it.

Orbital information for the Earth and probe is read in by the program during the run as orbital elements (a, e, i, M_o, ω, Ω). This information coupled with a variable time from epoch (also read in) is converted to (x,y,z) coordinates, in which form the Earth and probe position and velocity are mapped in time. The geometry of M, ω, and Ω are indicated in Figure 8. Note that M is a mean anomaly.

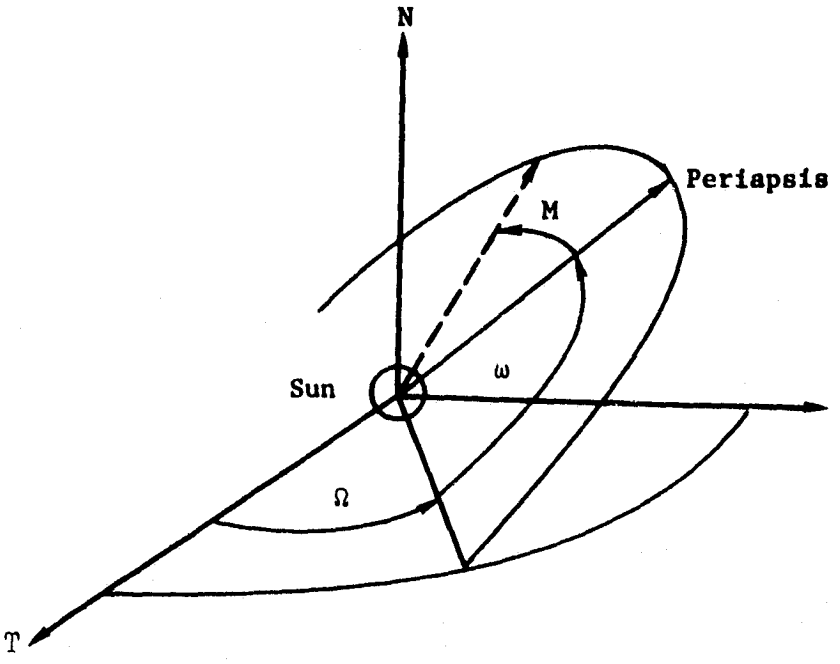

Figure 8. Orbital elements.

3.4 Preliminary Results

For comparison studies, a baseline case was selected and variations of individual parameters made around the baseline. For reasons discussed later, only range and range-rate observations were used in the baseline case. The following parameters were chosen for the baseline case:

Earth Elements: $(1.5 \times 10^8$ km, 0.02, 5.7°, 0°, 0°, 45°)

Probe Elements: $(3.914 \times 10^8$ km, 0.9928461, 90°, 0°, 180°, 90°)

(Aphelion at Jupiter, perihelion at 4 solar radii)

σ_u (self-gravity process noise) = 10^{-8} m/sec^2 (10^{-9} g)

σ_{J_2} **(process noise on** J_2**)** = 0

Start of estimation : Perihelion - 40 hrs

End of estimation: Perihelion + 40 hrs.

The above probe elements embody current thinking in trajectory design for this mission. The elements represent an aphelion at Jupiter which is used in a close swingby to create a highly eccentric polar orbit with perihelion occurring at four solar radii.

The estimation procedure is chosen to start and end at a far enough distance so that no J_2 information is lost. The times, ±40 hours, correspond to perifocal angles of ±137° and a distance from the sun of 29 solar radii (0.14 AU).

The self-gravity noise level is chosen to correspond to a nominal level of drag-free performance.

A large number of simulation runs were performed. The measure of goodness of any particular parameter set or encounter geometry is chosen as the minimum σ for the error in the estimated value of J_2. The behavior of σ_{J_2} is plotted for the baseline case in Figure 9. The notation $\Delta\Omega = \Omega_{probe} - \Omega_{Earth}$ is used. The behavior of σ_{J_2} is shown for a significantly poorer geometry ($\Delta\Omega$ = 90°) in Figure 10 and for a slightly better one ($\Delta\Omega$ = 165°) in Figure 11.

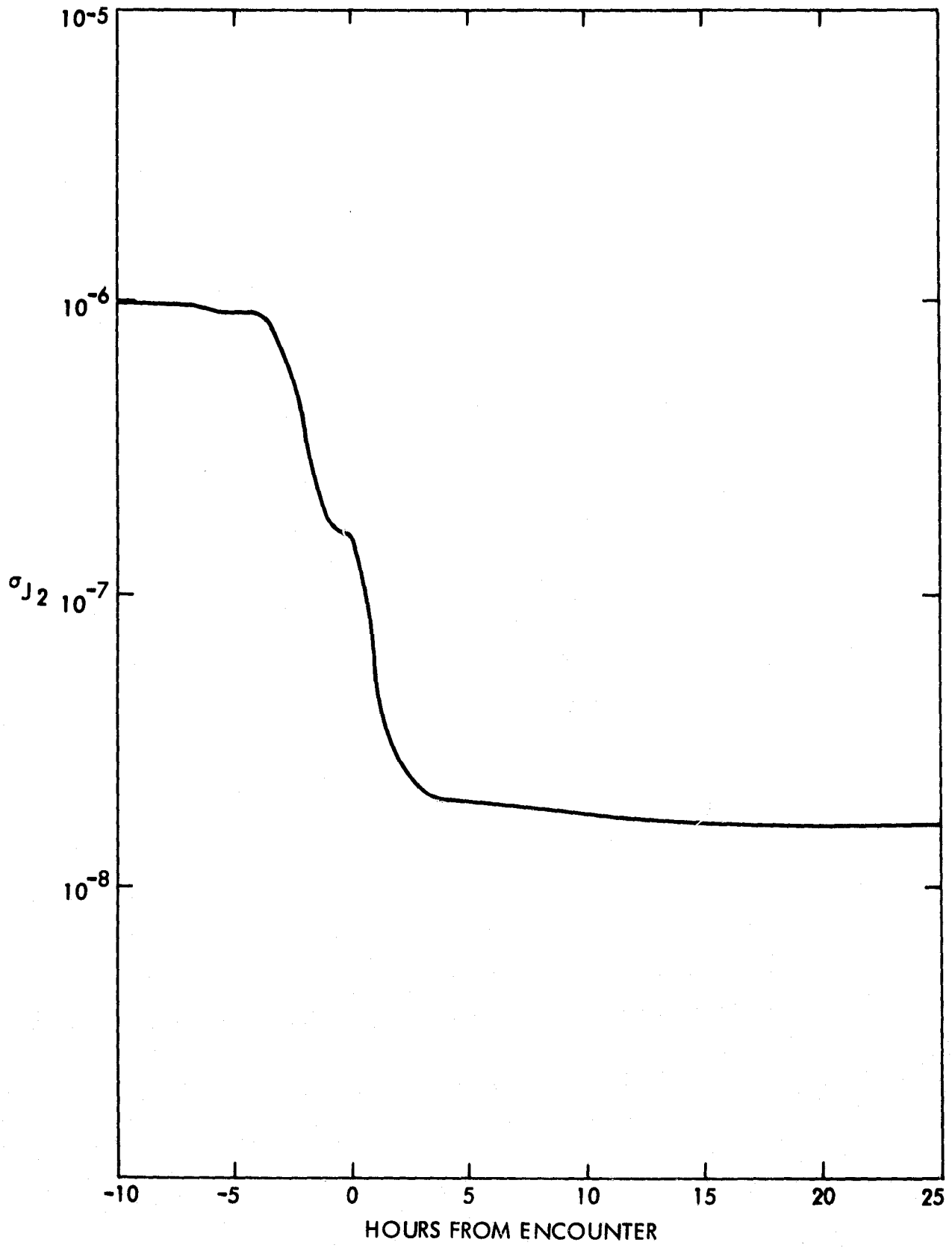

Figure 9. Behavior of σ_{J_2} under baseline conditions.

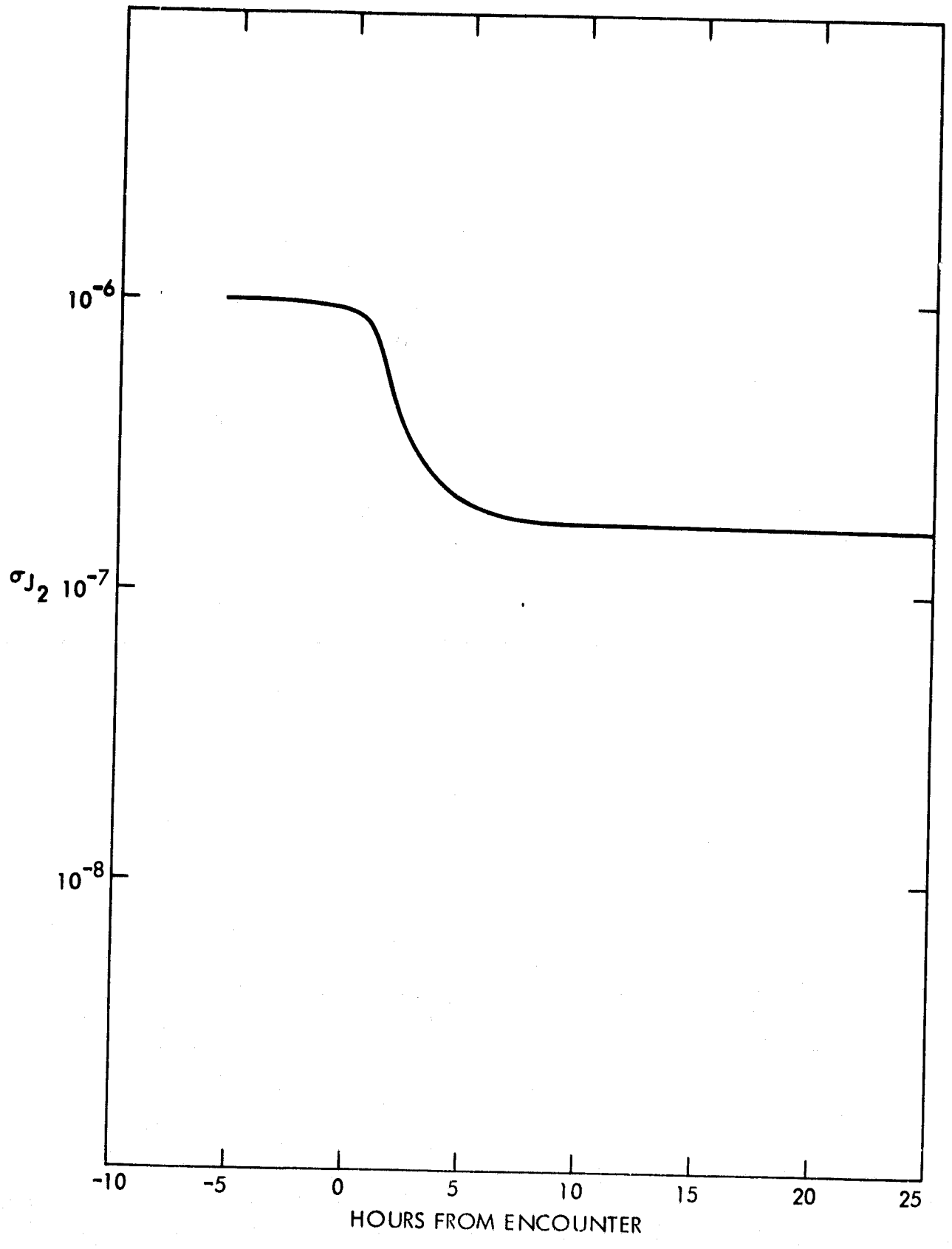

Figure 10. Baseline except $\Omega = 135^{o}$ ($\Delta\Omega = 90^{o}$).

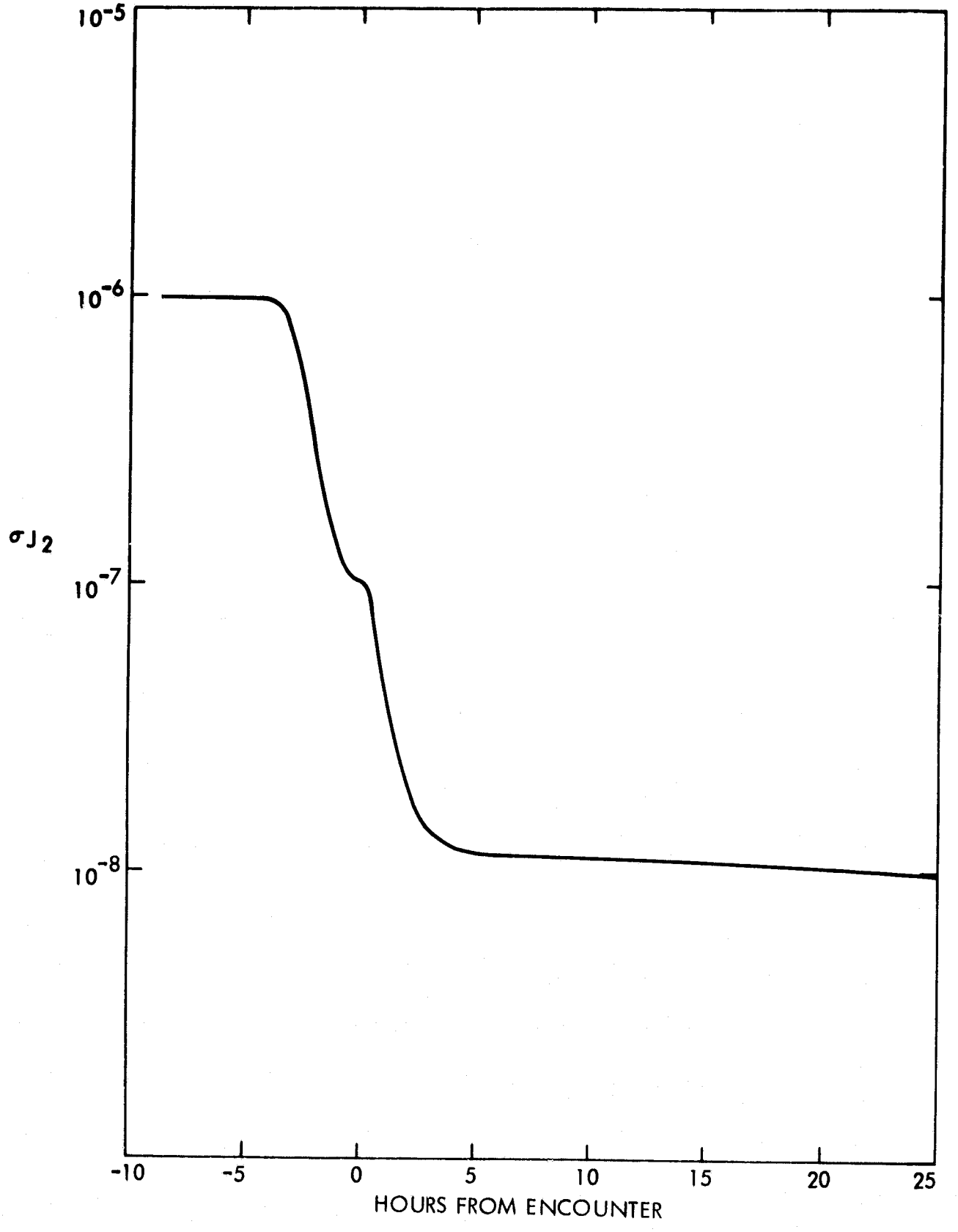

Figure 11. Baseline except $\Delta\Omega = 200^{\circ}$.

Some of the qualitative aspects of the estimation problem can be identified in these figures. The flattening of the curve for σ_{J_2} is indicative of a loss of estimation capability at that point. The flattening of the curve at encounter minus five minutes in Figure 9, for example, corresponds roughly to the probe's passage over a pole of the Sun. The very poor overall estimation behavior exhibited in Figure 10 can be attributed to observing the probe from a direction normal to the flight path for which there is no probe-induced doppler shift, and thus, no information for estimating J_2.

The poor behavior when perihelion occurs at the solar equator ($t = 0$ in Figure 9) might be attributed to one or more of the following reasons:

(a) Observability of J_2 is poor near the equator.
(b) There is no probe-induced doppler shift when the Earth and probe are in exact opposition, and thus no information for estimating J_2.
(c) The point of closest approach, which should be the point of greatest effect of J_2, occurs when J_2 cannot be extracted because of (a) or (b) above.

Figure 12 shows the behavior of σ_{J_2} as a function of $\Delta\Omega$; Figure 13 shows the behavior as a function of the probe's argument of perihelion; and Figure 14 as a function of probe inclination.

A study of Figure 13 indicates a significant improvement from the baseline case when the probe perihelion is moved away from the solar equator ($\omega = 180^{\circ}$) in either direction. Ordinarily, a change in ω would require a change in the line of apsides with a concomitant large energy cost. Fortunately, the Sun's polar axis is shifted approximately 7.25° from the normal to the ecliptic. Thus, by timing the approach correctly, a shift in ω of up to 7.25° may be obtained essentially for free. Referring to Figure 13 we see that a 7.25° shift to either side of 180° reaps most of the off-equator benefit available.

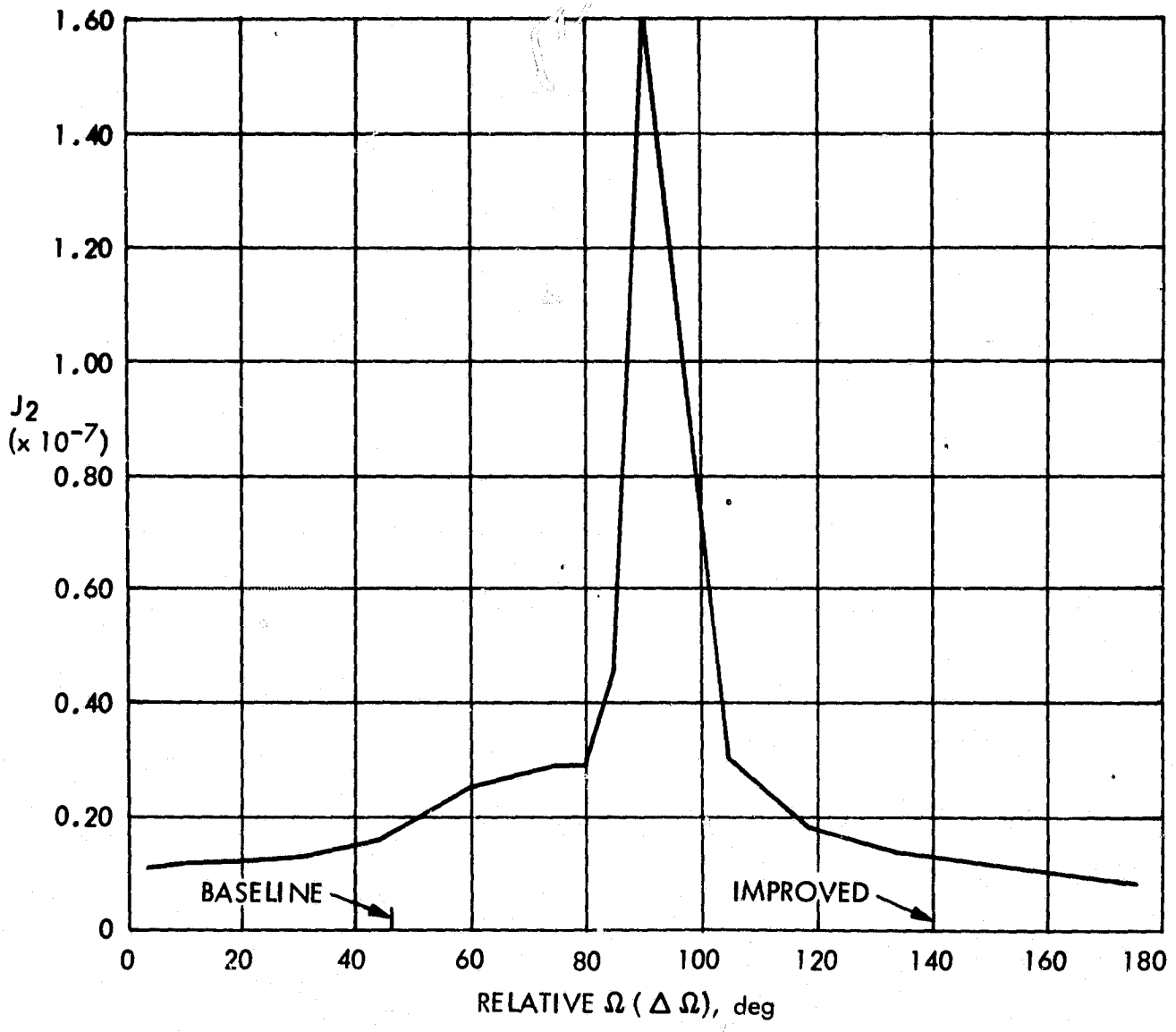

Figure 12. Final σ_{J_2} as a function of $\Delta\Omega$.

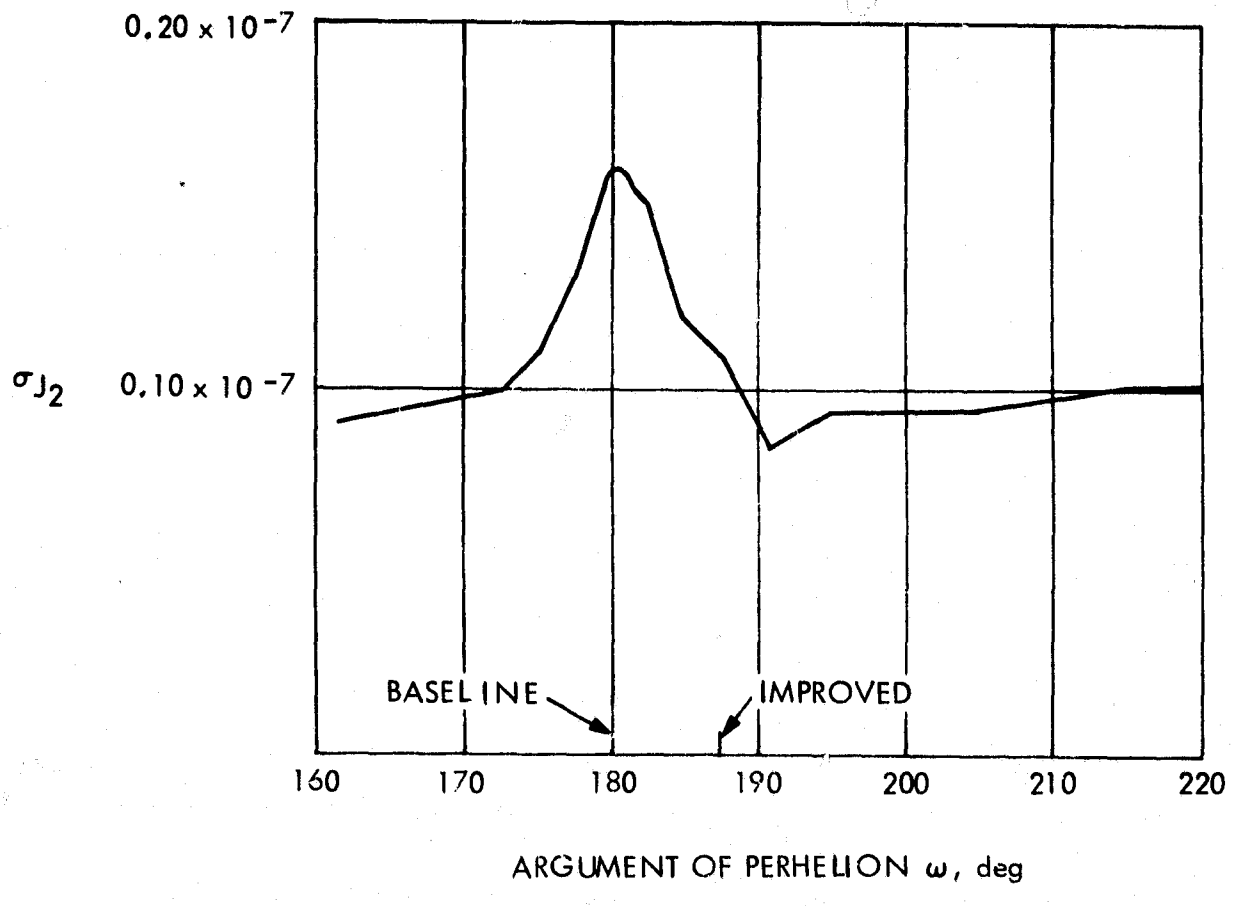

Figure 13. σ_{J_2} as a function of argument of perihelion.

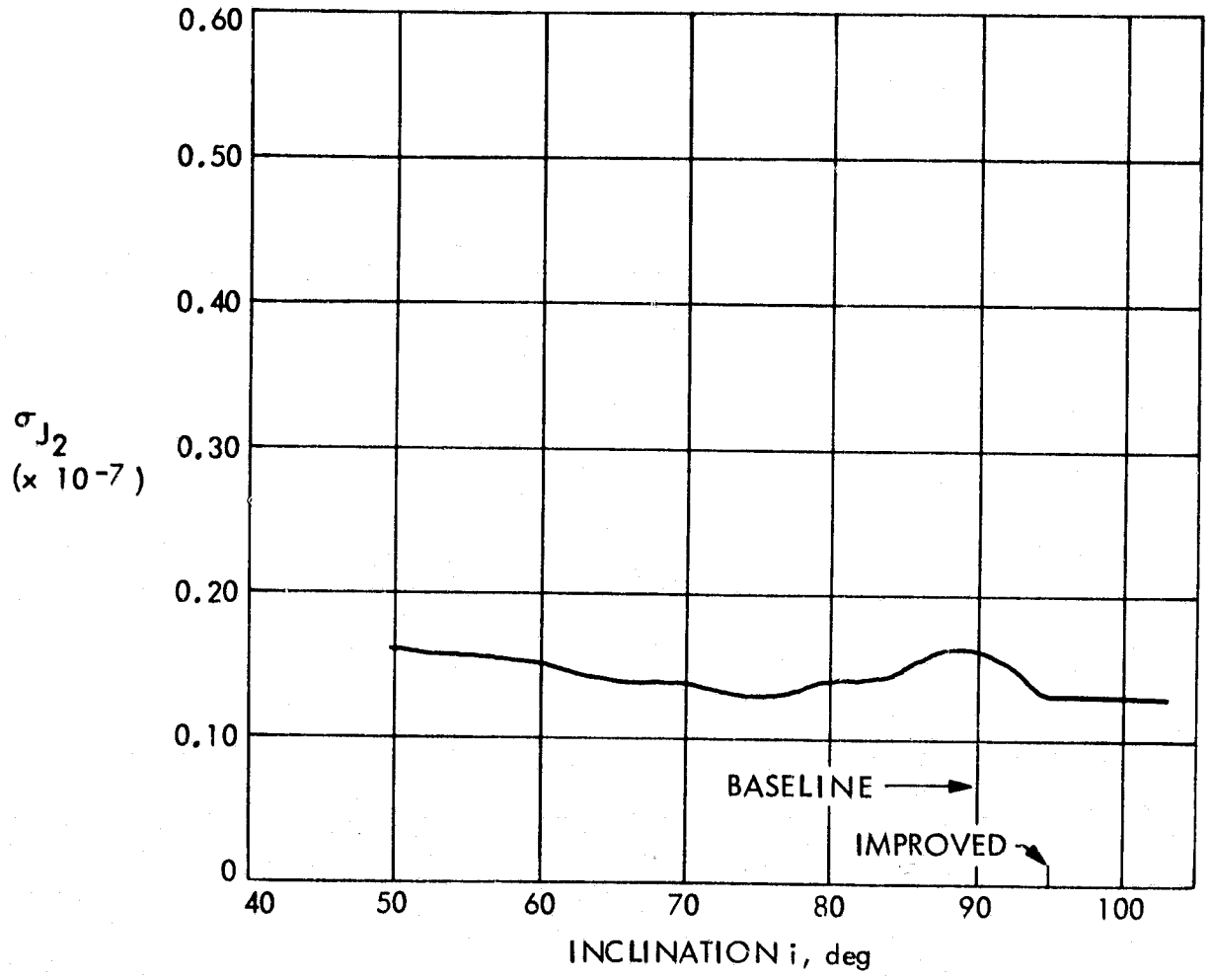

Figure 14. σ_{J_2} as a function of inclination.

Further comparison runs were performed for which perihelion was varied from 3 to 10 solar radii. The results from both the baseline and an improved parameter set ($i=82°$, $\omega=187°$, $\Delta\Omega=150°$) at various radii are shown in Figure 15.

Finally, the level of random acceleration noise was varied at several levels of doppler measurement accuracy. Results are presented in Figure 16 for the baseline case and in Figure 17 for the following improved geometry case:

Earth Elements: $(1.5 \times 10^8 \text{km}, 0.02, 7.25°, 0°, 0°, 90°)$

Probe Elements: $(3.914 \times 10^8 \text{km}, 0.9928461, 95°, 0°, 187.25°, 230°)$

We observe that in the left-hand portion of the graph, estimation performance is dominated by the doppler accuracy. On the right-hand portion, performance becomes strictly a function of the drag-free noise level. We note that unless $\sigma_{\dot{r}}$ can be brought below the approximate 0.4 mm/sec level(over 60 sec. integration periods) there is no level of drag-free performance which will allow estimation of J_2 to the 10^{-8} accuracy desired for this mission.

3.5 Comments

The initial version of the simulation program would not work. The estimated state diverged badly from the "true" state. An investigation of the gravitational forces involved and the method of propagating the equations of motion led to a solution to the problem and an insight into potential problems the mission software might encounter:

(a) Solar force terms had to include terms to $\ddot{\ddot{r}}$ in the discrete update,

(b) Time steps had to be relatively small (10 sec/step at perihelion),

(c) It was found that relativistic terms of order (v^4/c^4) generate accelerations of order 10^{-11} m/sec^2 at perihelion. Thus, the current JPL orbit determination program which neglects these terms might need to be

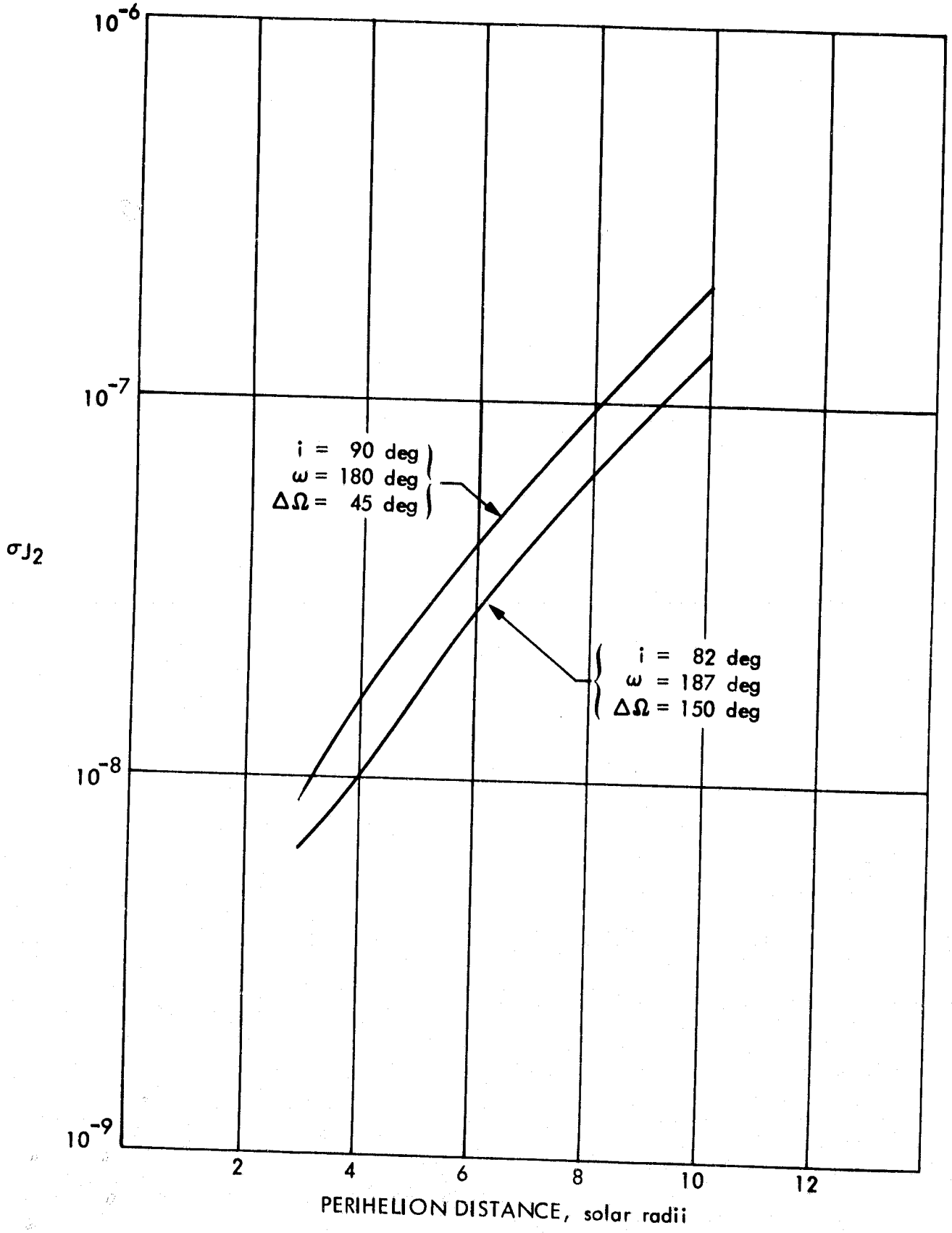

Figure 15. Minimum σ_{J_2} as a function of perihelion distance.

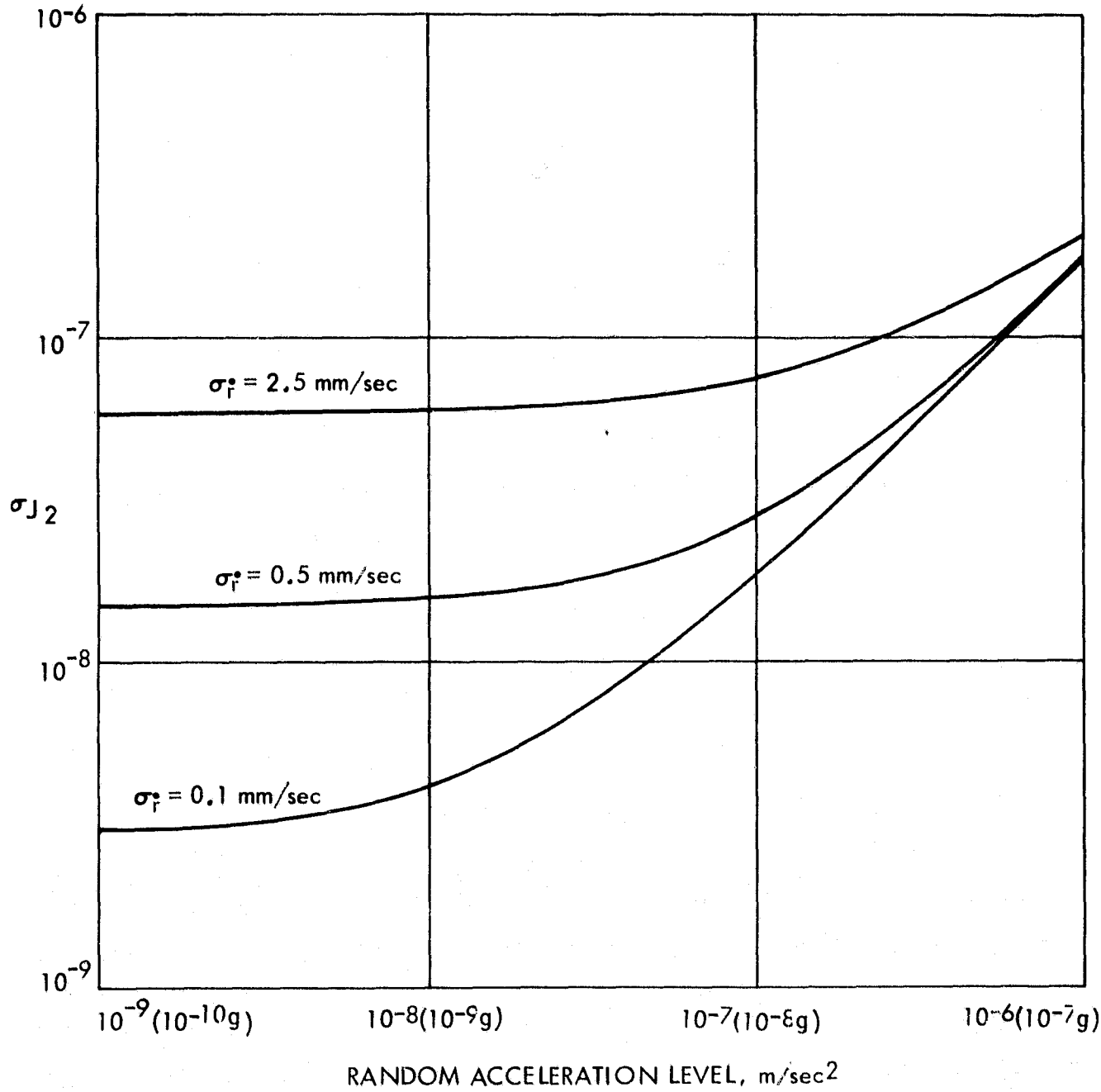

Figure 16. Minimum σ_{J_2} as a function of random acceleration level.

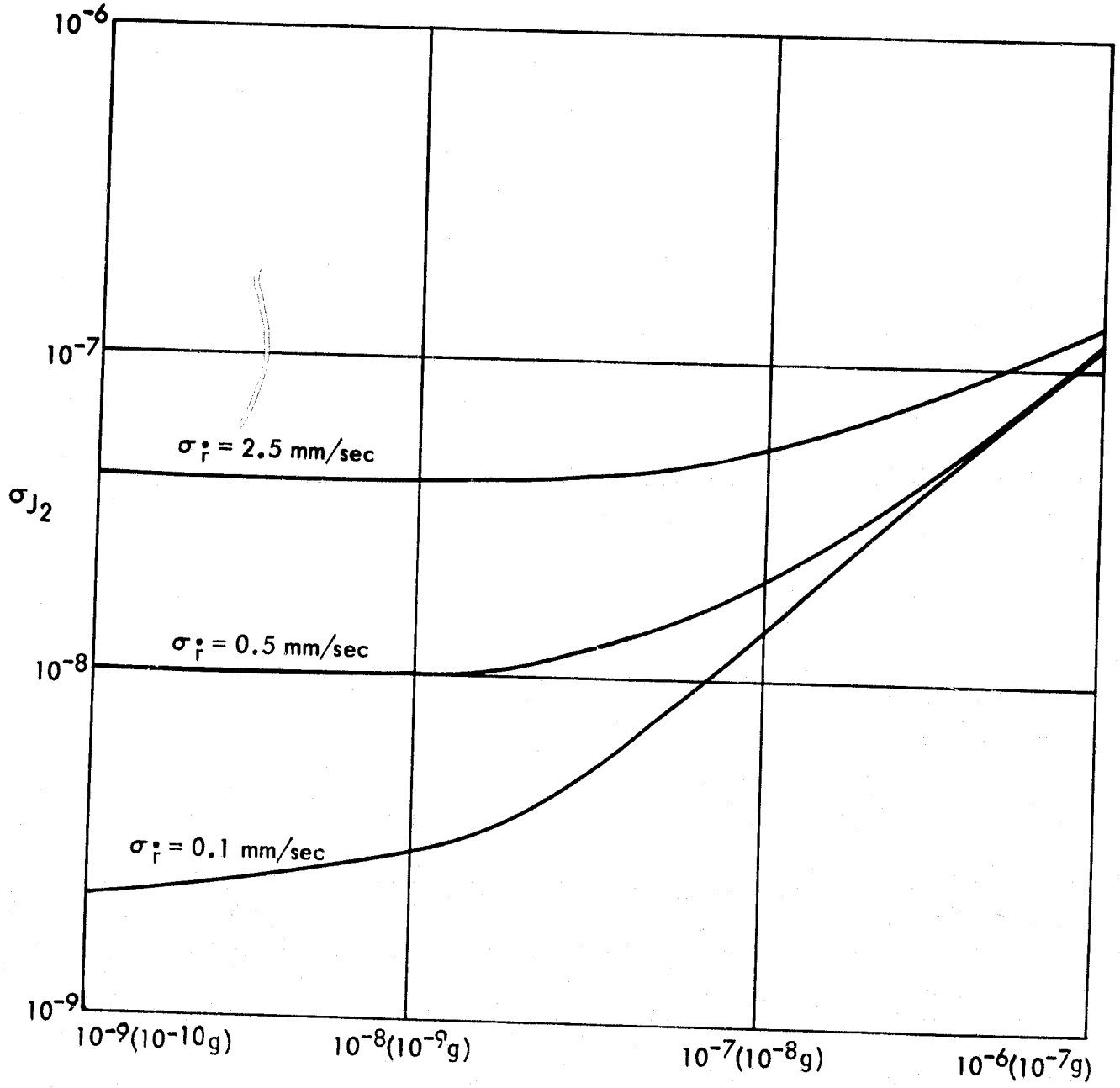

Figure 17. Minimum σ_{J_2} as a function of random acceleration level (improved geometry case).

updated to include them. We note that the peculiarities of this mission will likely require other changes. Before any changes are initiated, all mission requirements should be carefully investigated.

Initial trials indicated that angular measurements, either directly through VLBI or indirectly through doppler measurements, had very little influence on improving filter state estimates. A quick calculation gave an 8 km angular position resolution for ΔVLBI and a 75 km angular resolution from the doppler data. Since steady state position errors are of the order of a few hundred meters it became clear that currently available angular measurements will not be useful for tracking purposes. Thus, the balance of the testing was performed with only range and doppler as observables.

For the case of doppler data, the implication was that low declinations (for which the angular information vanishes) would not adversely affect the estimation results. This supposition was tested empirically and found to be true.

Because it is clear that the doppler data will be the dominant data type, special attention should be given to it in preparation for the mission. A possible problem area might be the doppler integration time requirement. For interplanetary missions no great change in the doppler signal is expected with averaging over a few minutes time. For the Solar Probe mission, this is not true — the spacecraft is moving very rapidly ($\sim$ 300 km/sec) in a rapidly changing gravitational environment. Thus, special doppler processing beyond simple averaging might be required. Furthermore, multiple, frequent, discrete accelerations of the drag-free thrustors at the 10^{-3} m/sec^2 level could seriously degrade or even impede doppler performance. In any case,

the extraction and processing of doppler data should be an item for early attention.

In the generation of the observations, two of the largest unmodeled error sources were included. These are station location errors and Earth ephemeris errors.

Station location errors were chosen from values consistent with currently known accuracies. In cylindrical coordinates these are of magnitude:[7]

Radial - 1 meter (1σ)

Longitudinal - 2 meter (1σ)

Spin axis - 10 meter (1σ)

It was found that station location errors of the above magnitudes did not adversely affect the estimation process until the larger values of self-gravitational disturbances were used.

Earth ephemeris errors to which the ephemeris providers will currently commit are as follows:[8]

Radial - 10 km (1σ)

Downtrack - 40 km (1σ)

Out-of-Plane - 70 km (1σ)

It was found that Earth ephemeris errors, even at levels only 1% of the above magnitudes, were extremely destructive to the estimation process. Over the approximately three days of perihelion encounter however, these errors will remain nearly unchanged. Thus, if the filter is expanded so that these terms are estimated, it is reasonable to believe that their deleterious effects will be overcome.

As can be seen from the above, there are many navigation aspects of a Solar Probe drag-free mission which need further attention. Even the current ideas concerning the baseline mission need examination. We note that nearly every variation from the current baseline gives some measure of improvement in the estimate of σ_{J_2}. Of course, as mentioned previously, there are other objectives to the Solar Probe mission, and the trajectory cannot be designed for J_2 estimation alone.

4. SELF-GRAVITY

Spacecraft self-gravity will be one of the largest perturbations of the drag-free system, with specific forces at the sensor on the order of 3×10^{-8} m/sec^2. There will also be time-varying changes in self-gravity due to articulated instruments, propellant expenditure, thermal distortion, etc. We must therefore devise some strategy to estimate or calibrate the self-gravity parameters to obtain the required accuracy, which may be as tight as 10^{-9} m/sec^2.

4.1 Mathematical Model

The spacecraft may be considered to be an assembly of masses at various positions about the drag-free sensor. Defining a coordinate system with the origin at the center of the sensor, consider one of the individual masses M_n at some position $\vec{r}_n$ from the sensor.

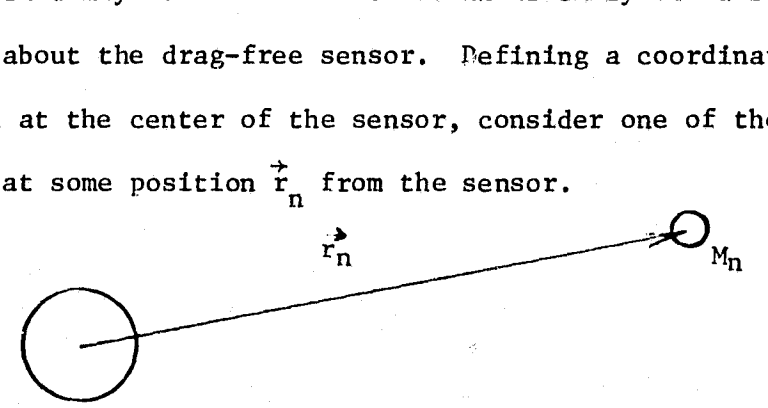

Drag-Free Sensor

The gravitational potential at the origin due to mass M_n is given by:

$$V_o(n) = \frac{GM_n}{|\vec{r}_n|} \tag{46}$$

Where G is the universal gravitational constant.

V_o is not useful in any direct way, but the next two derivatives (with respect to $\vec{r}_n$) are. These give us the acceleration (or specific force) $\vec{f}_n$ and the gradient of the acceleration $\vec{\vec{G}}_n$, as follows:

$$\vec{f}_n = \partial_{\vec{r}} \frac{GM_n}{|\vec{r}_n|} \tag{47}$$

$$\vec{\vec{G}}_n = \partial_{\vec{r}\vec{r}} \frac{GM_n}{|\vec{r}_n|} \tag{48}$$

Spatial variation of $\vec{\vec{G}}_n$ and higher order terms is negligible.

The total acceleration ($\vec{f}_i$) and gradient ($\vec{\vec{G}}_y$) at the sensor is just the sum of individual contributions:

$$\vec{f}_i = \sum_n \partial_{\vec{r}} \frac{GM_n}{|\vec{r}_n|} \tag{49}$$

$$\vec{\vec{G}}_y = \sum_n \partial_{\vec{r}\vec{r}} \frac{GM_n}{\vec{r}} \tag{50}$$

$\vec{f}_i$ and $\vec{\vec{G}}_y$ now represent the initial self-gravity and the gradient thereof. However, these parameters may change with time due to changes in mass or position.

A <u>change in mass</u> of an element will clearly produce a proportional change in that element's specific force, and the total change in self-gravity will be the sum of the individual contributions, or:

$$\Delta\vec{f}_i = \sum_n \frac{\Delta M_n}{M_n} \vec{f}_n \tag{51}$$

If mass M_n <u>changes position</u> by an amount $\Delta\vec{r}_n$ and the positional change is small enough so that $\vec{\vec{G}}_n$ is not significantly affected, then the total change in specific force at the sensor due to all motions can be written:

$$\Delta f_i = -\sum_n \vec{\vec{G}}_n \cdot \Delta \vec{r}_n \qquad (52)$$

It is possible to have relatively large motions for which $\vec{\vec{G}}_n$ changes appreciably, in which case we must integrate the quantity $\vec{\vec{G}}_n \cdot \vec{r}_n \, dr_n$ from the starting position to the final position.

Liquid propellants present the problem of simultaneous changes in mass and location. With a propellant level measurement α_p, the mass distribution and therefore the self-gravity should be determinable, or:

$$\Delta \vec{f}_i = \vec{f}(\alpha_p) \qquad (53)$$

The function $\vec{f}(\alpha_p)$ will not be a straightforward one, but some simplified modeling undoubtedly be done depending on specific applications. Tanks which do not have positive propellant control will need additional study in that the measurement of remaining fuel may be insufficient to completely determine the mass distribution.

Structure deformation and thermal distortion can be considered as an extension of the moving mass case. For each mass element, several spacecraft parameters (structure temperature and strain readings) may simultaneously affect that element's position. For small deflections, all effects can be considered independent and linear, so that we can write:

$$\Delta \vec{r}_n = \vec{\vec{S}}_n \cdot \vec{\alpha} \qquad (54)$$

Where $\vec{\vec{S}}_n$ is a tensor, specific to each mass element, which converts the overall set of readings $\vec{\alpha}$ into a positional change. $\vec{\vec{S}}_n$ should be determinable from configuration and thermal expansivity information.

combining (54) with (52), and defining a new tensor $\vec{\vec{D}} = \sum_n \vec{\vec{G}}_n \vec{\vec{S}}_n$, we can solve for $\vec{f}_i$:

$$\vec{f}_i = -\vec{\vec{D}} \cdot \vec{\alpha} \qquad (55)$$

Again, higher order terms will be negligible.

However, our assumption of independent effects may not be valid in that $\vec{\alpha}$ may overdetermine the spacecraft's mass distribution. In this case, we could derive $\vec{\vec{D}}$ from some sort of least squares fit, weighted with the assumed quality of the individual sensors. This has the virtue that if a sensor should fail, we would merely replace $\vec{\vec{D}}$ by command with a new best fit solution, containing a column of zeros corresponding to the failed sensor. In any case, $\vec{\vec{D}}$ might be improved by in-flight calibration.

4.2 Application

The first step in defining a drag-free system for a spacecraft is to determine what accuracy is required, and then develop an error budget to distribute the allowable error among the various sources. The report of the "Mass Attraction of TRIAD 1/ DISCOS"[7] provides a good example of this procedure.

An attractive alternative to the TRIAD method of extensive mass attraction calculations and tight manufacturing tolerances is the possibility of in-flight calibration. Since we are concerned only with the accuracy of the knowledge of spacecraft self-gravity and not trying to obtain any specific value, a program of ground tracking and prescribed spacecraft maneuvers could prove a more cost-effective way of determining the self-gravity parameters.

The drag-free system might be further simplified by elimination of the

$\vec{\vec{G}}_y \cdot \vec{y}$ term (in Chapter 2, eq. 14), where $\vec{y}$ is the proof mass displacement, through the use of an integral control scheme which would force the average value of $\vec{y}$ to zero. The same result can be gotten by tightening the deadband of the proof mass, thus reducing the impact of $\vec{\vec{G}}_y \cdot \vec{y}$; or $\vec{\vec{G}}_y$ can be reduced by careful compensation of the calculated gradient. In-flight gradient compensation would probably create more problems than it would solve.

For the Solar Probe spacecraft, the overall drag-free accuracy requirement will be in the range of 10^{-7} m/sec^2 to 10^{-9} m/sec^2. Proof mass charge and spacecraft self-gravity will be the main sources of drag-free uncertainty, so the following table has been generated assuming 10% of the total allowable error can be produced by a single item. Items are listed in approximate order of importance. The configuration used for this table was taken from Reference 8.

Figures 18 and 19 can be used to find the acceleration and gradient fields produced by a point mass at any distance. The tables give components in the radial direction; horizontal-horizontal components are half this value.

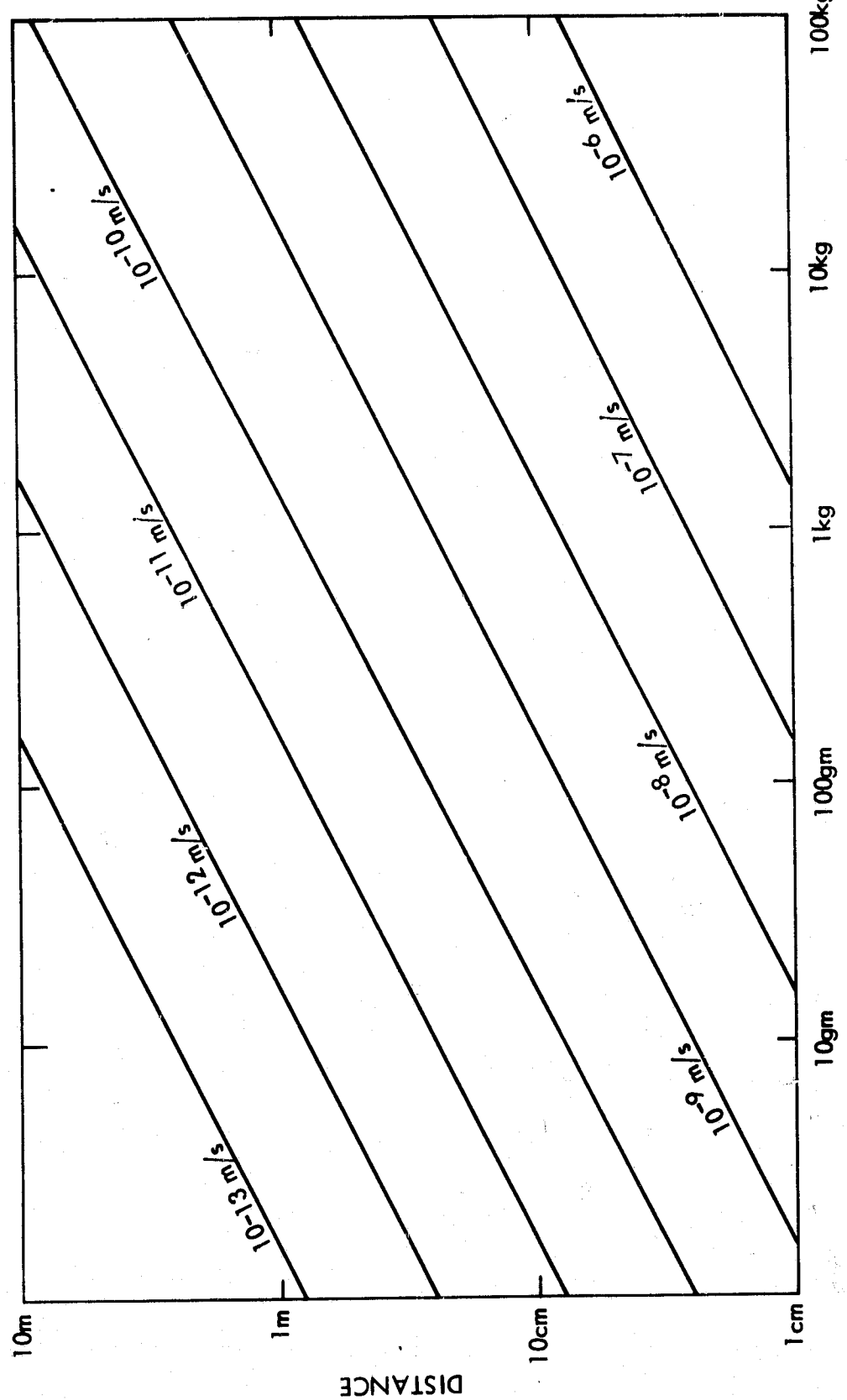

Figure 18. Specific force (acceleration) produced by mass.

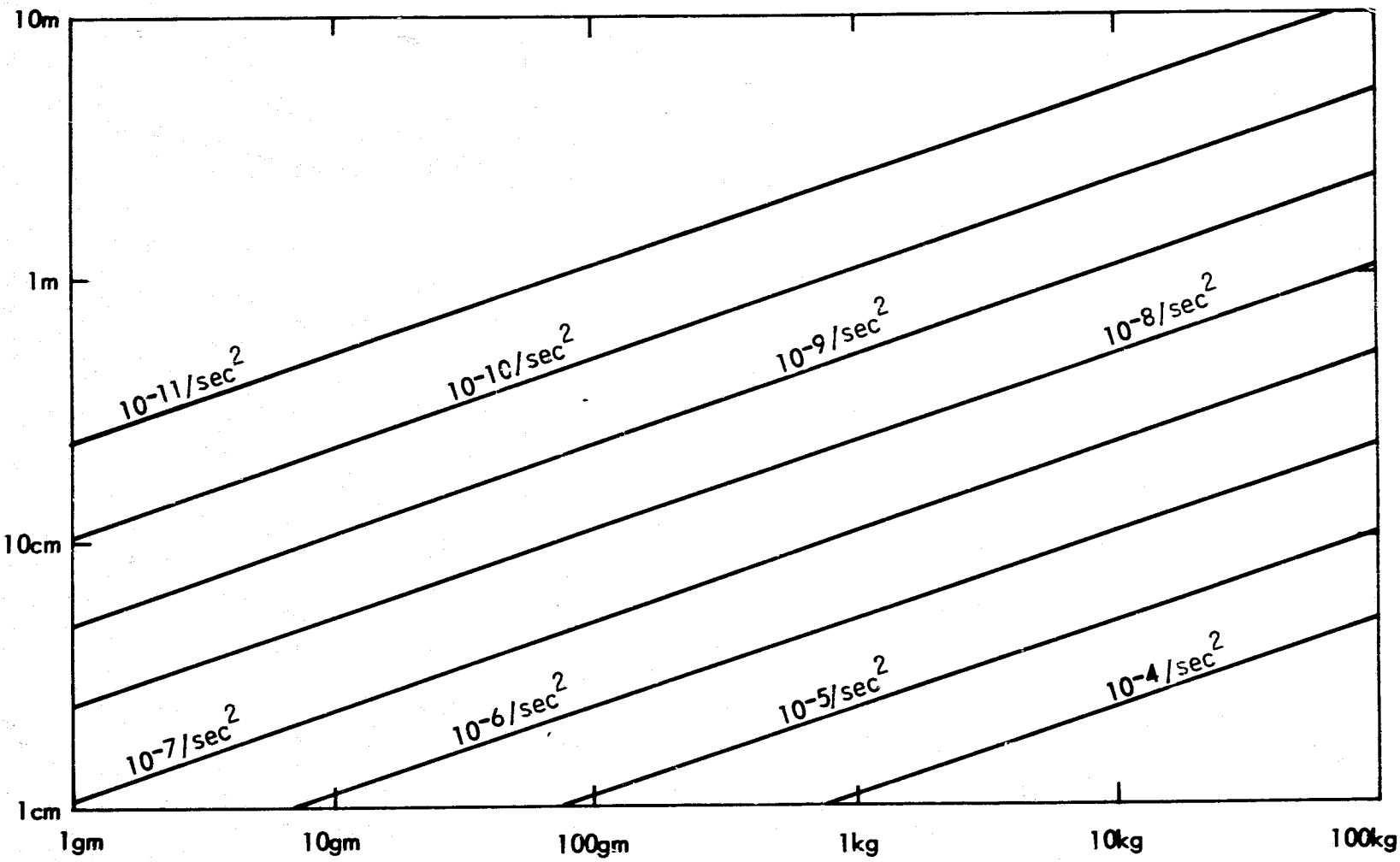

Figure 19. Gravity gradient produced by mass.

Accuracy	Factors
10^{-9} m/sec^2	• Less than 1% error allowed in calculating (or calibrating) self-gravity acceleration. • Articulations, deployment, etc., will have a major although easily accounted for impact on self-gravity specific force. No special sensors will be required. • Knowledge of propellant mass and location is critical; new methods of propellant measurement may be required. • Self-gravity gradient and proof mass position will be important. • Thermal distortion may have to be measured or predicted for a few critical elements of structure. • Spatial variation of the gradient could be important for large (5 mm or so) proof mass excursions.

10^{-8} m/sec^2

- Self-gravity acceleration must still be found, but a small scale analysis for a priori determination, or a short in-flight calibration period should be sufficient.
- Only some of the articulated instruments will have to be modeled, and even those will need only back-of-envelope definition.
- Propellant level must be tracked, but existing measurement techniques are adequate.
- Rough calculation of the gravity gradient should be accurate enough.

10^{-7} m/sec^2

- With a reasonably spherical pickoff housing, everything can be neglected.

The preceding list is a fairly generalized one, but some more specific requirements for Solar Probe have been calculated for 10^{-9} m/sec^2 accuracy. They are included here to give a feeling for the dynamic constraints on the spacecraft.

Antenna - must know orientation within 18 degrees.

Telescope - must know pointing position within 2 degrees.

Spin platform - must know position within 4 cm.

Structure thermal warpage - must know temperature of sensor support structure within 70 K.

Mass Loss - must know mass of main shield within 3.3 kg.

Propellant - must know mass within 1.5 kg and position within 9 mm. Existing techniques of measuring pressurant pressure or bookkeeping thruster firings may only be accurate to 8.7 kg. Positive propellant control, such as a diaphragm or bellows type tank, will be needed.

4.3 Summary of Self-Gravity

The inclusion of a drag-free sensor on a multipurpose spacecraft will not impose any harsh requirements on the design. Only the highest foreseeable level of drag-free accuracy will require a moderate amount of work and possibly some propellant tank development; otherwise existing techniques and simple analysis will suffice. Proof mass position and structure warpage are the only "fast" variables to be handled by the on-board estimator, and the chances are good that even these do not seriously impact the drag-free accuracy and may be dropped from consideration. All other parameters are "slow" and/or predictable, and can be handled in the ground estimator.

5. REFERENCES

1. Sonnabend, D., "Drag-Free Is So Necessary," JPL IOM 312/79.7-137, 11-12-79 (JPL Internal Document).

2. Goldstein, R., "Electrical Charging of Solar Probe Drag-Free Mass," JPL IOM, 9-25-79 (JPL Internal Document).

3. Purvis, C., "Jupiter Probe Charging Study," NASA Technical Paper 1263, Jan. 1979.

4. Neugebauer, M., et al., "The Energetic Particle Environment of the Solar Probe Mission," JPL Publication 78-64, Sept. 1, 1978.

5. Peck, E.R., Electricity and Magnetism, 1953, McGraw.

6. Sonnabend, D., "Drag Free Air Density Instrument," Guidance and Control Lab., Stanford University, April 1978.

7. Flemming, A.W., and Tashker, M.G., "Mass Attraction of TRIAD1/DISCOS," Stanford University, SUDAAR 445, 9-72.

8. "Solar Probe Final Report of 1979 Study," JPL Doc. No. 715-5 (JPL Internal Document).

NASA—JPL—Coml., L.A., Calif.